Effect of Out-Tunneling Leakage and Electron-Hole Asymmetry on Modulation Response of Semiconductor Double Tunneling-Injection Quantum Dot Lasers

Saurav Kar

Thesis submitted to the faculty of the
Virginia Polytechnic Institute and State University in
partial fulfillment of the requirements for the degree of

Master of Science
In
Materials Science and Engineering

Levon V. Asryan, Chair
Louis J. Guido
Mariusz K. Orlowski

August 3, 2017
Blacksburg, Virginia
Keywords: quantum dot lasers, semiconductor lasers

Copyright 2017, Saurav Kar

Effect of Out-Tunneling Leakage and Electron-Hole Asymmetry on Modulation Response of Semiconductor Double Tunneling-Injection Quantum Dot Lasers

`

Saurav Kar

Abstract

In this thesis, our primary objective was to theoretically analyze the real world modulation bandwidth of a DTI QD laser and this was done by analyzing the effect of out-tunneling leakage of carriers from QDs, and by analyzing the effect of electron-hole asymmetry on the device characteristics. We are confronted with the following results:

1) **Effect of Out-Tunneling Leakage on Modulation Bandwidth in Double Tunneling Injection Quantum Dot Lasers**

To purely focus on this effect, the conditions of instantaneous carrier exchange between the OCL and QW (on each side of the structure) and tunneling injection into QDs are assumed and closed-form analytical expressions for modulation bandwidth are obtained. The relative decrease in modulation bandwidth, due to this effect, in a DTI QD laser (from plots of modulation bandwidth vs j on increasing w_{out}) is then shown to be small, and at ranges of injection currents of operational interest, nearly negligible. Consequently, it is shown that the DTI laser is a robust device in terms of sensitivity to out-tunneling leakage i.e. much effort need not be paid in suppressing this phenomenon.

2) **Effect of Electron-Hole Asymmetry on Modulation Bandwidth of Double Tunneling Injection Quantum Dot Lasers**

On analyzing the effect of electron-hole asymmetry on the device characteristics of a DTI QD laser, it can be noted (from plots of modulation bandwidth vs injection current) that there is no reduction in the maximum modulation bandwidth i.e. electron-hole asymmetry does not indicate a reduction in the effectiveness of such a DTI design. This is shown to occur as the maximum modulation bandwidth depends on both, the effective differential non-stimulated recombination time as well the photon lifetime in the optical cavity. The photon lifetime being much smaller than the former acts as the dominating factor, and hence we see no appreciable change in the maximum modulation bandwidth.

In the course of this analysis, we also see that the actual condition i.e. that of electron hole asymmetry is closer, among the cases of symmetry, to symmetry assuming hole parameters rather than electron parameters. As such, in cases where electron-hole symmetry must be used (in order to facilitate numerical simplifications), a recommendation of this study is to use hole parameters instead.

Effect of Out-Tunneling Leakage and Electron-Hole Asymmetry on Modulation Response of Semiconductor Double Tunneling-Injection Quantum Dot Lasers

Saurav Kar

General Audience Abstract

In this age of internet and optical communications, semiconductor lasers have a profound impact on the way we interact with our world. They act as intermediaries converting digital signals into optical pulses (in order to be transmitted) and then back into digital code. Understandably, the maximum speed at which these lasers can encode and decode information limits the speed of this entire communication network. This speed can be defined as the modulation bandwidth.

A new design, the double tunneling-injection (DTI) quantum dot (QD) laser shows considerable promise, however its modulation bandwidth under real world operating conditions was yet to be analyzed. The aim of this thesis was to then theoretically analyze the real world modulation bandwidth of this new semiconductor laser design. This was done by analyzing the effect of unwanted leakage of carriers (out-tunneling) from the active region (Quantum Dots), and by analyzing the effect of electron-hole asymmetry on the device characteristics.

The relative decrease in modulation bandwidth, due to leakage of carriers, in a DTI QD laser is then shown to be nearly negligible. Consequently, it is shown that the DTI QD laser is a robust device in terms of sensitivity to out-tunneling leakage, i.e., much effort need not be paid in suppressing this phenomenon.

On analyzing the effect of electron-hole asymmetry on the device characteristics of a DTI QD laser, it is shown that there is no reduction in the maximum modulation bandwidth, i.e., electron-hole asymmetry does not indicate a reduction in the effectiveness of such a design.

Thus, this analysis reiterates the fact that DTI QD lasers indeed show incredible potential to drastically improve modulation bandwidth and must be investigated further.

Acknowledgments

I would like to express my heartfelt appreciation and gratitude to the following people for their encouragement and support:

- My advisor, Dr. Levon V. Asryan, for all his guidance and advice throughout my M.S. course. His unparalleled knowledge and keen insight in this subject have taught me a lot. I have taken away many life lessons from my time with him.

- Dr. Mariusz Orlowski for the many discussions that I have had with him. His class has been challenging, but rewarding. His comments and suggestions regarding my thesis have been invaluable.

- Dr. Louis Guido for his valuable time on discussions and comments about my research.

- Our Graduate Coordinator, Kim Grandstaff, for all her encouragement, support and for answering every question I could ever ask. Her advice, though not technical has been critical to my life and well-being here in Blacksburg.

- My colleagues Srilekhya Meda and Anastasia Yakusheva, for being amazing friends, for their invaluable advice and being a sounding board for so many of my ideas. Thank you for not growing tired of me.

I would like to thank all the members of the MSE Department for being an integral part of my life here in Blacksburg.

I would like to acknowledge the U.S. Army Research Office (Grant No. W911-NF-13-1-0445) for funding of this work.

My most sincere thanks to my family, without whose love and support I would never have been here.

Table of Contents

Abstract ii

General Audience Abstract iii

Acknowledgements iv

Table of Contents v

List of Figures vii

List of Abbreviations ix

Chapter 1. Introduction **1**

1.1. Lasing in semiconductors 1

1.2. Homojunction lasers 2
1.3. Heterostructure lasers 2
1.4. Double heterostructure lasers 2

1.5. Low-dimensional semiconductor lasers 3
1.5.1. Quantum well lasers 3
1.5.2. Quantum wire lasers 4
1.5.3. Quantum dot lasers 5

1.6. Modulation of optical response 6

1.7. Need for suppressing parasitic recombination 7

1.8. Tunneling-injection 8
1.9. Double tunneling-injection 8

1.10. Electron-hole asymmetry 9

1.11. Objective 9
References 11

Chapter 2. Effect of Out-Tunneling Leakage on Modulation Bandwidth in Double Tunneling Injection Quantum Dot Lasers 18

Summary 18
2.1. Introduction 18

2.2. Theoretical model 19
2.2.1. Main assumptions 20
2.2.2. Rate equations 21
2.2.3. Small signal analysis....22
2.3. Discussion 23

2.4. Conclusion 29

Appendix A: Analysis of equations 31
Appendix B: Equations (2.1)-(2.3) at the steady state 38
Appendix C: Small-signal analysis 39
References 42

Chapter 3. Effect of Electron-Hole Asymmetry on Modulation Bandwidth of Double Tunneling Injection Quantum Dot Lasers 47

Summary 47
3.1. Introduction 47

3.2. Theoretical model 48
3.2.1. Main assumptions 48
3.2.2. Modified rate equations model 48
3.3. Effect of electron-hole asymmetry on differential gain and non-stimulated differential recombination time 49

3.4. Discussion 52

3.5. Conclusion 57

Appendix D: Steady state solutions 58
Appendix E: Modulation response 59
Appendix F: Proof that L^{min} is unaffected by the electron-hole asymmetry....63
Appendix G: Differential gain for L tending to (i)L^{min} and (ii)infinity 65
Appendix H: Expressions for non-stimulated differential recombination time 68
References 69

Conclusions 70

List of Figures

Fig. 1.1. (a) absorption of photon from valence to conduction band and (b) stimulated emission of photon. 1

Fig. 1.2. Energy band diagram of a DHL structure. 3

Fig. 1.3. Density of states in (a) bulk semiconductor (3D), (b) quantum well (2D), (c) quantum wire (1D), and (d) quantum dot (0D). 4

Fig. 1.4. Three possible modes for the hetero-epitaxial growth: (a) Frank-van der Merwe (FM), (b) Volmer-Weber (VW), and (c) Stranski-Krastanow (SK). 5

Fig. 1.5. Schematic of a simple optical fiber communication system 6

Fig. 1.6. Schematic view of parasitic recombination (denoted as nonlasing) in an energy band diagram of a conventional QD laser. 7

Fig. 2.1. Schematic side view and energy band diagram of a double tunneling-injection (DTI) QD laser. (Reprinted with permission from fig. 1 of [30]). 19

Fig. 2.2. Modulation bandwidth vs Injection current density (j_0) for various out-tunneling coefficients. 23

Fig. 2.3. Modulation bandwidth vs out-tunneling coefficient (w_{out}) for various injection current densities. 24

Fig. 2.4. Modulation bandwidth vs off–resonance energy (Δ) for various injection current densities. 25

Fig. 2.5. Schematic depicting off–resonance energy (Δ) for a DTI QD laser. 26

Fig. 2.6. Modulation bandwidth vs out-tunneling coefficient (w_{out}) for various off–resonance energies (Δ). 26

Fig. 2.7. Modulation bandwidth vs out-tunneling coefficient (w_{out}) for various cavity lengths (L). 27

Fig. 2.8. Modulation bandwidth vs out-tunneling coefficient (w_{out}) for various QD surface densities (Ns). 28

Fig. 2.9. Modulation bandwidth vs cavity length and QD surface density in an ideal double tunneling-injection quantum dot laser. (Reprinted with permission from fig. 5 of [37]). ……28

Fig. 2.10. Modulation bandwidth vs out-tunneling coefficient (w_{out}) for various values of line broadening (δ). ……29

Fig. 2.11. Conduction band diagram of the electron-injecting side of the structure. ………32

Fig. 3.1. Steady state level occupancies (*f*) vs cavity length (L) for various situations. …52

Fig. 3.2. Modulation bandwidth vs dc injection current density (j_0) for three cases electron-hole symmetry using (i) electron parameters, (ii) hole parameters and (iii) for electron-hole asymmetry. ……53

Fig. 3.3. Reciprocal optimum injection current vs cavity length squared (L^2) of QDs for three cases electron-hole symmetry using (i) electron parameters, (ii) hole parameters and (iii) for electron-hole asymmetry. ……54

Fig. 3.4. Differential gain (G^{dif}) vs cavity length (L) for three cases electron-hole symmetry using (i) electron parameters, (ii) hole parameters and (iii) for electron-hole asymmetry. ……55

Fig. 3.5. Fig (a) Reciprocal effective differential non-stimulated recombination time vs cavity length (L) of QDs for three cases electron-hole symmetry using (i) electron parameters, (ii) hole parameters and (iii) for electron-hole asymmetry.
Fig (b) along with the reciprocal photon lifetime, plotted in log scale. ……56

List of Abbreviations

DHL	Double-heterostructure laser.
cw	Continuous Wave. Indicative of the fact that the laser produces a continuous optical beam as opposed to a pulse.
LED	Light emitting diode.
DTI	Double tunneling-injection.
QW	Quantum well. Implies 1-D quantum confinement.
QWR	Quantum wire. Implies 2-D quantum confinement.
QD	Quantum dot. Implies 3-D quantum confinement.
LCC	Light-current characteristic.
OCL	Optical confinement layer.
MBE	Molecular beam epitaxy. An epitaxy method for thin-film deposition of single crystals.
MOCVD	Metalorganic chemical vapor deposition. It is a chemical vapor deposition method used to produce single or polycrystalline thin films. In contrast to molecular beam epitaxy (MBE) the growth of crystals is by chemical reaction and not physical deposition
SK	Stranski-Krastanow growth. A self-organized mode of quantum-dot growth.

Chapter 1

Introduction

1.1. Lasing in Semiconductors

Semiconductor lasers use electroluminescence i.e. radiative recombination of electrons and holes (stimulated by electrical pumping) to generate light. The fact that this typically takes place in a p-n junction, makes these devices relatively small and compact. Their low cost of production and high efficiency makes them the device of choice in a variety of applications.

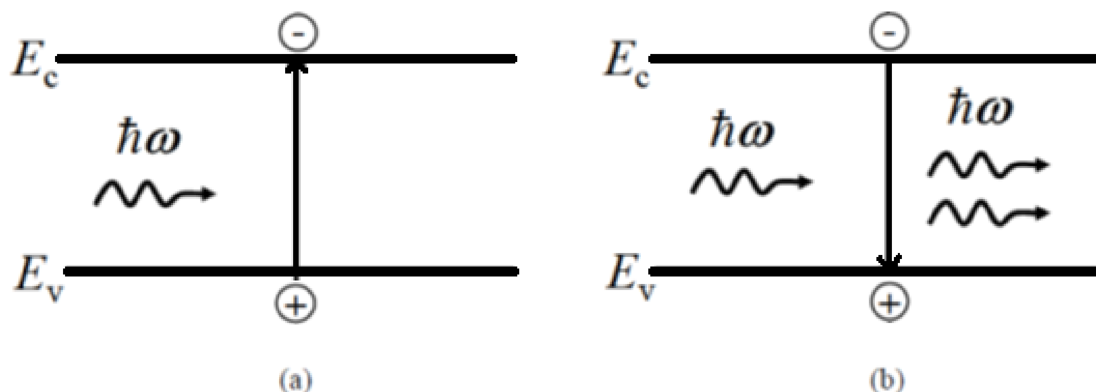

Fig. 1.1. (a) absorption of photon from valence to conduction band and (b) stimulated emission of photon

Fig. 1.1 depicts schematically the process of photon absorption and luminescence in a semiconductor. For stimulated emission first an electron-hole pair is created i.e. an electron must first be excited from the valence band into the conduction band. This pair could be generated by the absorption of an incident photon on the semiconductor or by injection of carriers. Recombination of this excited electron hole pair occurs due to interaction with incident photons leading to the creation of one more photon which has the same energy and wavelength as the incident photon.

Electrons are distributed according to the Fermi-Dirac statistics which predict that under thermal equilibrium the probability of occupation of higher energy conduction band states is less than the probability of occupation of lower energy valence band states. Consequently, there are more electrons in the valence band than in the conduction band. In such a scenario, most of the incident photons are absorbed. If on the other hand, the number of conduction band (higher energy state) electrons is more than the number of lower energy valence band electrons, a case termed as population-inversion, more photons are emitted than absorbed i.e. the net stimulated emission is more than the absorption and optical amplification takes place.

A major part in creating a laser reduces to creating a population inversion. Semiconductor p-n junctions are readily manipulated in this regard by injecting currents, which provide high energy carriers in the confined region, generating the necessary conditions for lasing. As the population inversion is achieved using an injection current, such lasers are also referred to as injection lasers. Also, as lasing occurs over a p-n junction the term laser diode is also used.

1.2. Homojunction lasers

As early as the late 1950's and the early 1960's the potential for using semiconductors in lasing was sensed [1]-[3].A wave of fundamental breakthroughs came in 1962. The electroluminescence spectrum narrowing was first observed in GaAs diode at 77 K [4]. Using this, Hall *et al.* [5] devised the first semiconductor laser at GE Schenectady. This was an infra-red laser with a lasing wavelength of 842 nm and a spectral width of 1.5 nm.

Nick Holonyak[6] and others [7, 8] in the very same year went on to observe coherent emissions in infrared and visible light.

These early attempts at semiconductor lasers suffered though from one fundamental problem, that continuous wave (CW) lasing was operable only at cryogenic temperatures. This was due to the excessively high threshold current densities that came about as a result of using the same material on either side of the p-n junction. The homojunction had to be replaced.

1.3. Heterostructure lasers

The possibilities for these devices in lightwave communication looked promising except for the fact that at this stage, semiconductor laser were still cryogenically operated. Room temperature operation was critical.

It was soon becoming apparent that was only one real solution to the high threshold current density caused by using a homojunction. Replace it by a suitable heterojunction. The only challenge remaining was that of fabrication. That was solved as soon as new techniques of crystal growth and epitaxial technologies were developed.

1.4. Double heterostructure lasers

By the 1970's it had been well established by Alferov [9], Hayashi and Panish [10] that double heterostructure lasers (DHLs) could continuously operate at room temperature. The evolution of this idea can however be traced back to 1963 when Alferov and Kazarinov [11] and Kroemer [12] first proposed what was then a novel idea, the DHL.

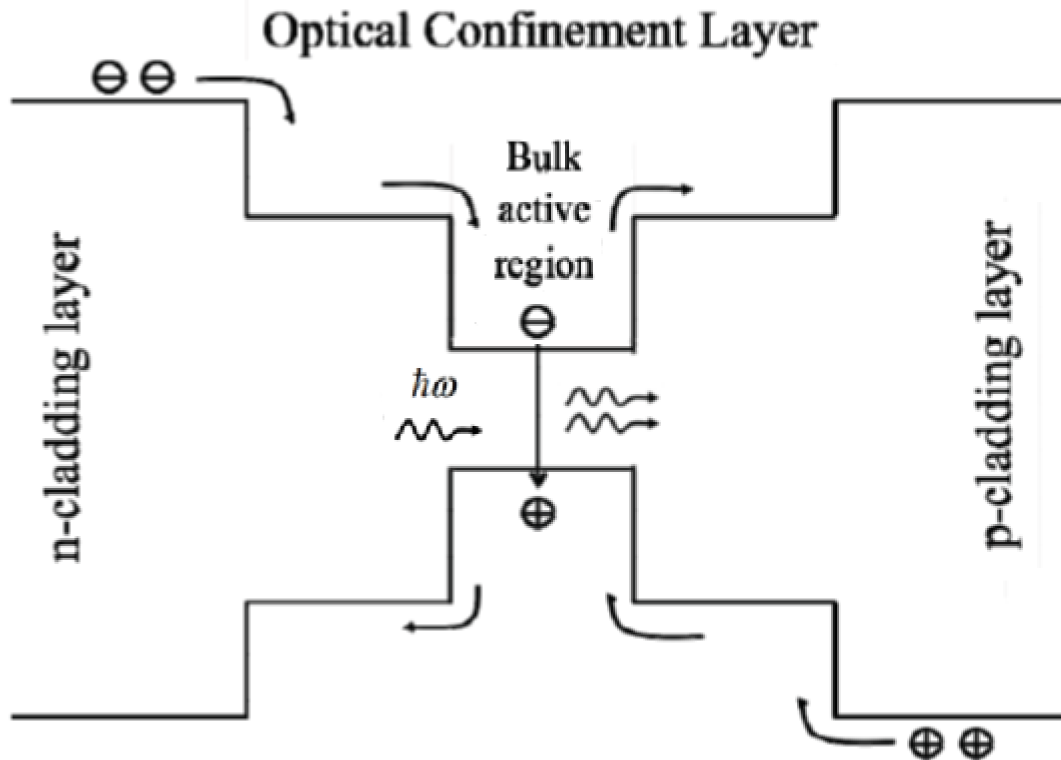

Fig. 1.2. Energy band diagram of a DHL structure

Fig. 1.2 shows a basic DHL structure. The idea of operation is essentially simple. The electrons and holes are to be confined in the active region, while the emitted photons are confined within the OCL. The objective is to reduce the lasing threshold with this strategy of separate confinement. The narrow bandgap active region is sandwiched by larger bandgap layers. This is what causes the electron and hole confinement. The OCL has a higher refractive index than the cladding layers. This effectively forms a waveguide and optical confinement is achieved. With this design, for the first time, room temperature CW lasing was achieved.

1.5. Low dimensional semiconductor lasers

1.5.1. Quantum-well lasers

From basic quantum mechanics it was already know that dimensionality plays a significant role in changing the density of states. The first semiconductor lasers didn't try and exploit this phenomenon. Simply bulk material was used where there was no quantum-mechanical confinement in any direction. Part of this stemmed from the fact that at that time, the techniques to reduce band thickness to close to the de Broglie wavelength didn't exist.

Dingle *et al.* [13, 14] was one of the first to attempt and observe quantum confinement in AlGaAs-GaAs-AlGaAs semiconductor heterostructures with an ultrathin GaAs layer. In 1975, Van Der Ziel *et al.* [15] and then later in 1978, Dupuis *et al.* [16] showed that quantum effects

could effectively be harnessed, coining the term quantum well (QW). Finally, with major improvements in molecular beam epitaxy (MBE), in 1982 Tsang [17], achieved what was then the lowest threshold current density using a graded index separate confinement heterostructure.

Then came the quantum cascade laser. Proposed initially in 1971 by Kazarinov and Suris [18]-[20], the idea was to create a semiconductor super-lattice and trigger stimulated emission using resonant electron tunneling between the quantized states. Limited by the technology of the time, this was experimentally verified more than 20 years later in 1994, by Faist and Capasso *et al.* [21, 22].

Alferov *et al*. [23, 24] brilliantly noticed that a short period variably spaced super-lattice would effectively bind the QW and then went on to show that in the GaAs-AlGaAs double heterostructure, separate confinement QW lasers, j_{th} would be about 52 A/cm^2 . Under optimal conditions, this would further drop to 40 A/cm^2 – by far the lowest j_{th} and it would remain so even till the late 1990s.

1.5.2. Quantum wire lasers

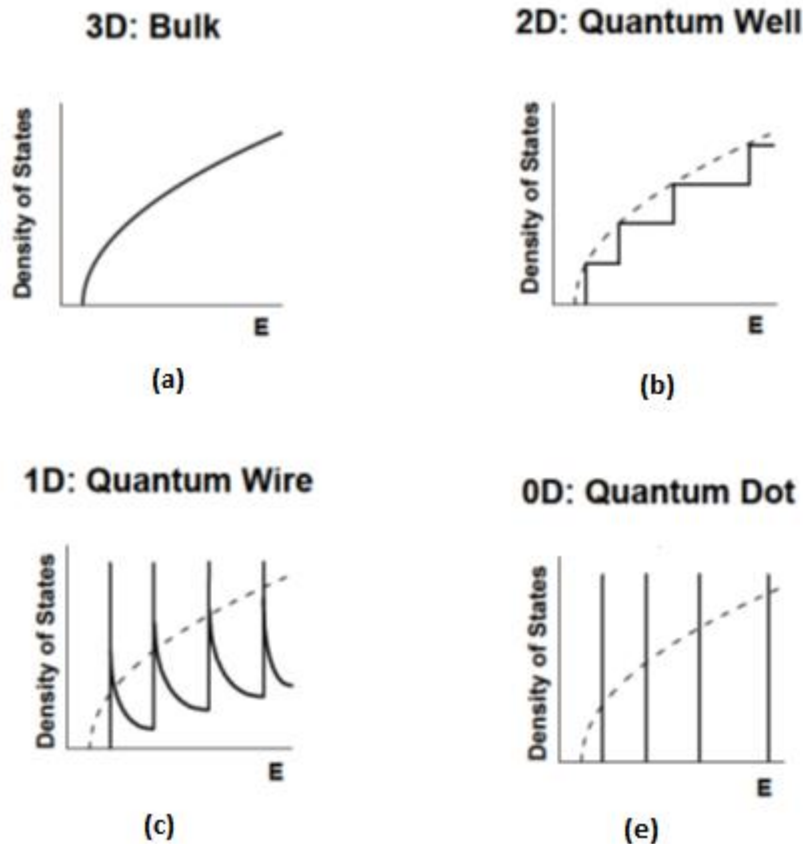

Fig. 1.3. Density of states in (a) bulk semiconductor (3D), (b) quantum well (2D), (c) quantum wire (1D), and (d) quantum dot (0D).

Fig. 1.3 shows the density of states as a function of dimensionality. We see that with on decreasing dimensionality, the density of states function changes from parabolic in 3-D to a delta function in 0-D. Till this point, the change in the threshold current had been brought about by reducing dimensionality, using confinement in just one direction. By extension, further confinement, owing to the nature of density of states would further reduce the thermal spread of carriers over energy states.

In 1982, Arakawa and Sakaki [25] proposed QWR and QD lasers, and went on to simulate QWRs by using a magnetic field, to create an additional degree of confinement in a DHS laser. As expected, an increased temperature stability was observed. In quantum wires (QWR), the density of states is a decreasing function [Fig. 1.3(c)] but in QDs, the density of states being a delta-function. This should imply that there be absolutely no thermal spread [Fig. 1.3(d)]. Theoretically, then the temperature stability should be infinite.

1.5.3. Quantum dot lasers

It was the self-organized Stranski-Krastanow (SK) growth mode that heralded a new age of devices. In an SK mode growth, crystal monolayers are grown one over the other. A lattice mismatch is intentionally introduced. The ever accumulating strain (due to the addition of layers) causes the layers to eventually break away beyond a critical thickness and start forming tapering 3-D islands. These are our quantum dots. Compared to other growth techniques, this method ensures largely defect free QDs. Although the problem of an unwanted 2-D starting layer, necessary to begin epitaxial growth, remains. This layer is termed the wetting layer [26]-[29].

For the monolayer deposition, first molecular beam epitaxy (MBE) and then metalorganic chemical vapor deposition (MOCVD) was used [30]. Ledentsov *et al.* [31] used MBE grown InAs-GaAs QD structures in an optically pumped laser. About the same time Kirstädter *et al.* [32] and Egorov *et al.* [33] reported the first room temperature QD laser diodes.

Alferov *et al.* [34] set the next bar by using MOCVD now bringing down the current density to $j_{th} = 150$ A/cm^2.

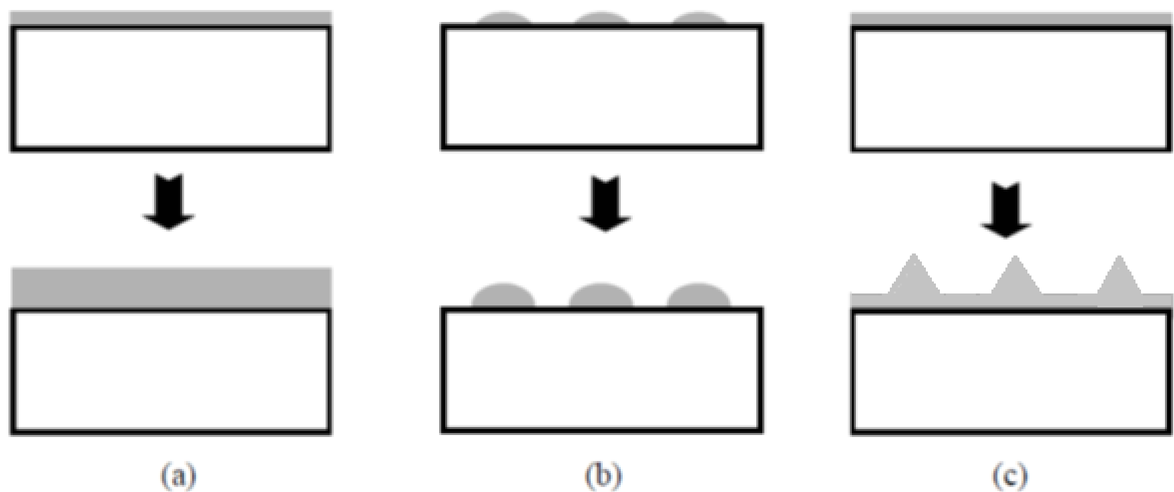

Fig. 1.4. Three possible modes for the hetero-epitaxial growth: (a) Frank-van der Merwe (FM), (b) Volmer-Weber (VW), and (c) Stranski-Krastanow (SK).

Fig. 1.4. schematically showing the various growth modes used.

In 1996, Asryan and Suris [35] calculated a threshold current density below 10 A/cm^2 at room temperature for an optimized QD lasers for a QD size dispersion restricted to 10%. This was an assumption made as the QDs themselves varied highly in structure and shape which leads to a significant variation in quantum confinement energy. Ustinov *et al.* [36]-[37] and then Zhukov *et al.* [38] brought down that threshold current density to 63 A/cm^2 using vertically coupled QDs.

In the year 2000, Park *et al.* [39] using QD structures, finally achieved something previously calculated, a threshold current density of around 19 A/ cm^2.

1.6. Modulation of optical response

In a semiconductor laser, simply by alternating the pump current, we can modulate the optical response. And thus, this presents a potential for data transfer and optical communication. But their use is dictated by not only the static response of a laser, but also by the speed with which the device can respond to the change in current injection.

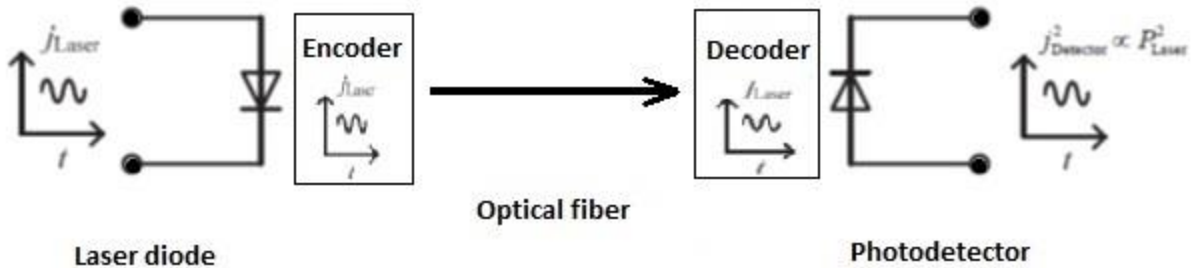

Fig. 1.5. Schematic of a simple optical fiber communication system (dealt with in greater detail under fig. 1.6 of [40])

Fig. 1.5. schematically depicts an optical fiber communication system. The laser diode takes up the role of a transmitter. It acts as an injection laser and converts electrical input to optical signals. As an input signal to the laser, the directly-modulating bias current causes a corresponding change in the laser optical output power and thus the information is transmitted. In such a lightwave system, the highest frequency (i.e., the modulation bandwidth), at which the modulation is still efficient, determines the amount of information that will be transmitted per unit time. For a non-return-to-zero binary format digital system, the maximum transmitted data rate (bit rate) is approximately twice the small-signal harmonic modulation bandwidth [41]. Hence, understanding the response of a semiconductor laser to a small time-harmonic modulating pump current is important for successful applications of semiconductor lasers in high-speed communication systems.

Typical optical data transmission using a typical single-mode silica fiber occurs on 1.3 µm wavelength for short distance communications (to minimize fiber dispersion) and 1.55 µm for long range (due to the minimum attenuation). And hence a large interest exists on lasers emitting in this wavelength range. The materials used for these applications include InGaAsP/InP, InGaAs/AlGaAs, InGaAs/GaAs and InAs/GaAs [42].

The first room-temperature 1.3 µm QD lasing was realized under pulse-current injection [43], and then the cw operation was also demonstrated [44]. Room temperature cw 1.5 µm lasing was also realized using either GaAs [45] or InP [46] as the substrate.

1.7. Need for suppressing parasitic recombination

Development of the QD laser has been rapid, but many issues remain that need to be resolved. One is that of the temperature sensitivity of the threshold current density, occurring because of the parasitic recombination outside QDs [47]. Another is the sub linearity of the light-current characteristic (LCC) [48].

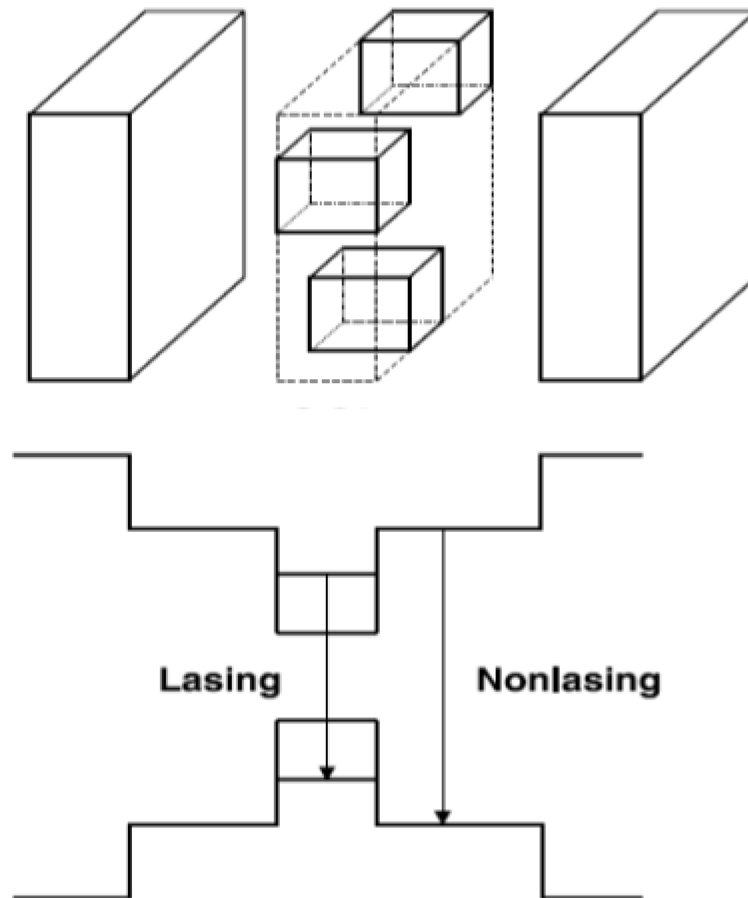

Fig. 1.6. Schematic view of parasitic recombination (denoted as nonlasing) in an energy band diagram of a conventional QD laser.

Fig. 1.6. shows a conventional QD laser heterostructure. Parasitic recombination of carriers is a mechanism of temperature dependence present in all semiconductor lasers, but in QD lasers at room temperature, it is the primary cause. Recombination arises primarily from carriers residing in layers adjacent the active medium, in what is called as the optical confinement layer (OCL). At room temperature, injected carriers from the cladding layer into the OCL essentially develop an equilibrium with the carriers in the QDs. Therefore, a large occupation of electron and hole levels in QDs implies an appreciable population of both electrons and holes in the bulk OCL itself. It is these carriers (in the bulk OCL), whose population is temperature-dependent, that gives rise to a recombination current not contributing to the lasing.

1.8. Tunneling-injection

In 1996 a new idea gained ground that was designed to reduce hot carrier effects - tunneling-injection of electrons in single and multiple QW lasers [49]. Hot carrier effects also reduce gain and increase Auger recombination [50, 51] To reduce this, here it was proposed that electrons injected from the cladding layer be first thermalized in a bulk volume (3D) and thus be rendered "cold". These electrons would then, due to low barrier thickness, tunnel into the QWs. For tunneling-injection in QW lasers (emitting at 0.98 μm) increased modulation bandwidth and lower chirp and temperature dependence of threshold current density was observed.

The same principle can be applied to QD lasers injecting electrons from the QW into the QDs [52]-[54]. In such a device although increased small-signal modulation bandwidth and lower temperature sensitivity of the threshold current density was noted, bipolar carrier density and consequently parasitic recombination still remained on the hole-injecting side.

Tunneling-injection of electrons into QDs was then first reported for an InP substrate based, InAs QD laser [55]. In the natural evolution of this idea, resonant tunneling was proposed [56] by longitudinal optical phonons, from bulk to the excited QD states.

1.9. Double tunneling-injection

It was not long before in [57]-[59], that to reduce recombination outside QDs still occurring on the hole injecting side, tunneling-injection of holes as well into QDs was suggested. There would now be two separate QWs. It was theorized in [57] that parasitic recombination, if completely suppressed, would then make the device characteristic temperature in excess of 1500 K.

In [60]-[63] experimental validation of the ideas described in [57]-[59] of injection of both electrons and holes by tunneling into QDs was attempted and the resulting device parameters compared with those found for a conventional QD laser. It was found that tunneling-injection can efficiently improve the uniformity of QDs by selecting the QDs of the 'right' size, and the carrier collection in QDs can also be improved [60]. With the tunneling-injection of both electrons and

holes, the highest experimentally obtained ground-state gain for a single-layer InAs QD laser was found, observing ground-state lasing for the first time in a short-cavity device [61]. Symmetrical gain shape and a smaller refractive index change at the peak gain wavelength were then found for a tunneling-injection QD laser [63].

1.10. Electron – hole asymmetry

While consistent device design modifications such as lowering dimensionality and incorporating tunneling-injection have improved performance by many orders of magnitude, systematic numerical modelling errors have so far created variations between the actual observed parameters and the theoretical model.

It is often implicitly assumed that electron and hole parameters are equal, in order to simplify procedures and calculations. It is however well known that they are not. Electron and hole level occupancies obtained self-consistently were shown to be different in [64]. Owing to this inherent asymmetry, there are variations in actual device performance parameters, from those theoretically calculated using models in which only one set of parameters are used. In this regard, studies have previously been conducted for semiconductor quantum-well lasers[65]-[68] showing that there are indeed inaccuracies generated as a result, however many such studies for quantum dot lasers[69] are yet to be conducted.

Hence, to truly validate the effectiveness of the DTI QD design, the degree of deviation of actual device characteristics owing to electron hole asymmetry needs to be assessed.

1.11. Objective

Dynamic properties of early QD lasers [25], was often modelled with a very basic two-equation model [70]-[72]. It was found that theoretically, QD lasers with a reasonably size distribution of QDs, could achieve a modulation bandwidth of 60 GHz [73], which galvanized further experimental research into this field.

The main challenge to the experimental testing of such structures is that these designs are challenging to grow, but initial attempts at already shows improvements in device characteristics. Experimentally, it was found that the highest stage $\omega_{-3\text{ dB}}$ (– 3 dB bandwidth is used for modulation bandwidth in diode lasers) is only 7.5 GHz (in a conventional single-QD-layer laser) [74] and this lowering from the theoretical value was attributed primarily to hot carrier effects.

For lasers employing tunneling injection (in order to reduce hot carrier effects and for a 3-QD-layer laser), the maximum experimentally obtained value of $\omega_{-3\text{ dB}}$ was found to be around 25 GHz (see [75]) and while this a considerable improvement, it is lower than that which is observed in a 4-quantum-well laser (40 GHz – see [76]), as well as the maximum theoretically predicted value. What has been realized finally is that these devices critically failed to suppress parasitic recombination. This is where the DTI QD laser comes in and becomes of interest as it is by design intended to reduce parasitic recombination as well as hot carrier effects.

Hence, due to the potential of DTI QD lasers, the modulation bandwidth of the output optical power by injection current must be investigated further. The primary idea behind this research is then to systematically study the theoretical behavior modulation bandwidth and the effect of various parameters on it in a DTI QD laser.

The structure of this thesis, the topics of the research, and the main results are elucidated below.

1) **Effect of out-tunneling leakage of carriers from the QDs into "foreign" QWs on the modulation bandwidth of a DTI QD laser (Chapter 2)**

A theoretical model, which takes into account the out-tunneling leakage of carriers was developed. It is shown that the out-tunneling has a limited effect on the modulation bandwidth $\omega_{-3\ \mathrm{dB}}$ of a QD laser. In order to purely focus on the out-tunneling, assumptions of instantaneous carrier capture from OCL to QW were made. The assumption of electron hole symmetry was also used in order to simplify and reduce the rate equations model.

2) **Effect of electron-hole asymmetry on the modulation bandwidth of a DTI QD laser (Chapter 3)**

The effect of inherently present electron hole asymmetry on modulation bandwidth is studied. A comprehensive theoretical model was developed in order to purely focus on this effect assuming instantaneous transfer of carriers from OCL to QW and no out tunneling.

REFERENCES

[1] N. G. Basov, B. M. Vul, and Yu. M. Popov, "Quantum-mechanical semiconductor generators and amplifiers of electromagnetic oscillations," *Sov. Phys. JETP,* vol. 10, pp. 416, 1960 [Translated from *Zh. Eksp. Teor. Fiz.* (U.S.S.R.), vol. 37, pp. 587-588, 1959].

[2] W. S. Boyle and D. G. Tomas, "Optical maser," U. S. patent 3 059 117, Oct. 16, 1962.

[3] N. G. Basov, O. N. Krokhin, and Yu. M. Popov, "Production of negative-temperature states in P-N junctions of degenerate semiconductors," *Sov. Phys. JETP*, vol. 13, pp. 1320-1321, 1961 [Translated from *Zh. Eksp. Teor. Fiz.* (U.S.S.R.), vol. 40, pp. 1879-1880, 1961].

[4] D. N. Nasledov, A. A. Rogachev, S. M. Ryvkin, and B. V. Tsarenkov, "Recombination radiation of gallium arsenide," *Sov. Phys. Solid State*, vol. 4, pp. 782-784, 1962 [Translated from *Fiz. Tverd. Tela*, vol. 4, pp. 1062, 1962].

[5] R. N. Hall, G. E. Fenner, J. D. Kingsley, T. J. Soltys and R. O. Carlson, "Coherent light emission from GaAs Junctions," *Phys. Rev. Lett.,* vol. 9, no. 9, pp. 366, Nov. 1962.

[6] N. Holonyak, Jr., and S. F. Bevacqua, "Coherent (visible) light emission from $Ga(As_{1-x}P_x)$ junctions,'' *Appl. Phys. Lett.,* vol. 1, no. 4, pp. 82-83, Dec. 1962.

[7] M. I. Nathan, W. P. Dumke, G. Burns, F. H. Dill, Jr., and G. Lasher, "Stimulated emission of radiation from GaAs p-n junctions," *Appl. Phys. Lett.*, vol. 1, no. 3, pp. 62-64, Nov. 1962.

[8] T. M. Quist, R. H. Rediker, R. J. Keyes, W. E. Krag, B. Lax, A. L. McWhorter, and H. J. Zeilger, "Semiconductor maser of GaAs," *Appl. Phys. Lett.*, vol. 1, no. 4, pp. 91-92, Dec. 1962.

[9] Zh. I. Alferov, V. M. Andreev, D. Z. Garbuzov, Yu. V. Zhilyaev, E. P. Morozov, E. L. Portnoi, and V. G. Trofim, "Investigation of the influence of the AlAs–GaAs heterostructure parameters on the laser threshold current and realization of continuous emission at room temperature," *Sov. Phys. Semicond.*, vol. 4, pp. 1573–1575, 1971 [Translated from *Fiz. Tekh. Poluprovodn.*, vol. 4, pp. 1826, 1970].

[10] I. Hayashi, M. B. Panish, P. W. Foy, and S. Sumski, "Junction lasers which operate continuously at room temperature," *Appl. Phys. Lett.*, vol. 17, no. 3, pp. 109-111, Aug. 1970.

[11] Zh. I. Alferov and R. F. Kazarinov, "Semiconductor laser with electric pumping," Inventor's Certificate 181737 [in Russian], Application No. 950840, priority as of Mar. 30, 1963.

[12] H. Kroemer, "Semiconductor laser with electric pumping," U.S. Patent 3 309 553, Aug. 16, 1963.

[13] R. Dingle, W. Wiegmann, and C. H. Henry, "Quantized states of confined carriers in very thin Al_xGa_{1-x} As–GaAs–Al_xGa_{1-x}As heterostructures," *Phys. Rev. Lett.*, vol. 33, no. 14, pp. 827–830, 1974.

[14] R. Dingle and C. H. Henry, "Quantum effects in heterostructure lasers," U.S. Patent 3 982 207, Sept. 21, 1976.

[15] J. P. van der Ziel, R. Dingle, R. C. Miller, W. Wiegmann, and W. A. Nordland, Jr., "Laser oscillation from quantum states in very thin GaAs–$Al_{0.2}Ga_{0.8}$As multilayer structures," *Appl. Phys. Lett.*, vol. 26, no. 8, pp. 463–465, Apr. 1975.

[16] R. D. Dupuis, P. D. Dapkus, N. Holonyak, Jr., E. A. Rezek, and R. Chin, "Room temperature operation of quantum-well $Ga_{(1-x)}Al_xAs$–GaAs laser diodes grown by metalorganic chemical vapor deposition," *Appl. Phys. Lett.*, vol. 32, no. 5, pp. 295–297, Mar. 1978.

[17] W. T. Tsang, "Extremely low threshold (AlGa)As graded-index waveguide separate confinement heterostructure lasers grown by molecular-beam epitaxy," *Appl. Phys. Lett.*, vol. 40, no. 3, pp. 217–219, Feb. 1982.

[18] R. F. Kazarinov and R. A. Suris, "Possibility of amplification of electromagnetic waves in a semiconductor with a superlattice," *Sov. Phys. Semicond.*, vol. 5, no. 4, pp. 707–709, 1971.

[19] R. F. Kazarinov and R. A. Suris, "Electric and electromagnetic properties of semiconductors with a superlattice," *Sov. Phys. Semicond.*, vol. 6, no. 1, pp. 120–131, 1972.

[20] R. F. Kazarinov and R. A. Suris, "Theory of electrical properties of semiconductors with superlattices," *Sov. Phys. Semicond.*, vol. 7, no. 3, pp. 347–352, 1973.

[21] J. Faist, F. Capasso, D. L. Sivco, C. Sirtori, A. L. Hutchinson, and A. Y. Cho, "Quantum cascade laser," *Sci.*, vol. 264, no. 5158, pp. 553–556, Apr.1994.

[22] J. Faist, F. Capasso, D. L. Sivco, C. Sirtori, A. L. Hutchinson, and A. Y. Cho, "Quantum cascade laser: An intersub-band semiconductor laser operating above liquid nitrogen temperature," *Electron. Lett.*, vol. 30, no. 11, pp. 865–866, May 1994.

[23] Zh. I. Alferov, A. I. Vasil'ev, S. V. Ivanov, P. S. Kop'ev, N. N. Ledentsov, M. E. Lutsenko, B. Y. Mel'tser, and V. M. Ustinov, "Lowering the threshold current density in GaAs– AlGaAs double-heterostructure separate-confinement quantum-well lasers ($J_{thr} = 52$ A/cm^2 , $T = 300$ K) by bounding the quantum well by a short-period variable-step superlattice," *Sov. Tech. Phys. Lett.*, vol. 14, pp. 782–784, 1988.

[24] Zh. I. Alferov, "Nobel lecture: The double heterostructure concept and its applications in physics, electronics, and technology," *Rev. Mod. Phys.,* vol. 73, no. 3, pp. 767–782, July 2001.

[25] Y. Arakawa and H. Sakaki, "Multidimensional quantum well laser and temperature dependence of its threshold current," *Appl. Phys. Lett.*, vol. 40, no. 11, pp. 939–941, Jun. 1982.

[26] K. Nishi, R. Mirin, D. Leonard, G. Medeiros-Ribeiro, P. M. Petroff, and A. C. Gossard, “Structural and optical characterization of InAs/InGaAs self-assembled quantum dots grown on (311)*B* GaAs,” *J. Appl. Phys.,* vol. 80, no. 6, pp. 3466–3470, Sept. 1996.

[27] R. Leon, Y. Kim, C. Jagadish, M. Gal, J. Zou, and D. J. H. Cockayne, “Effects of inter-diffusion on the luminescence of InGaAs/GaAs quantum dots,” *Appl. Phys. Lett.*, vol. 69, no. 13, pp. 1888–1890, Sept. 1996.

[28] A. Patanè, A. Polimeni, P. C. Main, M. Henini, and L. Eaves, “High-temperature light emission from InAs quantum dots,” *Appl. Phys. Lett.*, vol. 75, no. 6, pp. 814–816, Aug. 1999.

[29] J. S. Kim and I.-H. Bae, “Optical properties of wetting layer in InAs quantum dots at different growth temperatures,” *J. Korean Phys. Soc.*, vol. 42, no. 92, pp. S483–S486, Feb 2003.

[30] P. Bhattacharya, S. Krishna, J. Phillips, P. J. McCann, and K. Namjou, “Carrier dynamics in self-organized quantum dots and their application to long-wavelength sources and detectors, “ *J. Cryst. Growth,* vols. 227–228, pp. 27-35, July 2001.

[31] N. N. Ledentsov, V. M. Ustinov, A. Yu. Egorov, A. E. Zhukov, M. V. Maksimov, I. G. Tabatadze, and P. S. Kop’ev, “Optical-properties of heterostructures with InGaAs-GaAs quantum clusters,” *Semiconductors*, vol. 28, no. 8, pp. 832–834, Aug. 1994.

[32] N. Kirstädter, N. N. Ledentsov, M. Grundmann, D. Bimberg, V. M. Ustinov, S. S. Ruvimov, M. V. Maximov, P. S. Kop’ev, Zh. I. Alferov, U. Richter, P. Werner, U. Gösele, and J. Heydenreich, “Low threshold, large T_0 injection laser emission from (InGa)As quantum dots,” *Electron. Lett.*, vol. 30, no. 17, pp. 1416–1417, Aug. 1994.

[33] A. Yu. Egorov, A. E. Zhukov, P. S. Kop’ev, N. N. Ledentsov, M. V. Maksimov, and V. M. Ustinov, “Effect of deposition conditions on the formation of (In,Ga)As quantum clusters in a GaAs matrix,” *Semiconductors*, vol. 28, no. 8, pp. 809–811, Aug. 1994.

[34] Zh. I. Alferov, N. Y. Gordeev, S. V. Zaitsev, P. S. Kop’ev, I. V. Kochnev, V. V. Khomin, I. L. Krestnikov, N. N. Ledentsov, A. V. Lunev, M. V. Maksimov, S. S. Ruvimov, A. V. Sakharov, A. F. Tsatsul’nikov, Y. M. Shernyakov, and D. Bimberg, “A low-threshold injection heterojunction laser based on quantum dots, produced by gas-phase epitaxy from organometallic compounds,” *Sov. Phys. Semicond.*, vol. 30, no. 2, pp. 197–200, 1996.

[35] L. V. Asryan and R. A. Suris, “Inhomogeneous line broadening and the threshold current density of a semiconductor quantum dot laser,” *Semicond. Sci. Technol.*, vol. 11, no. 4, pp. 554–567, Apr. 1996.

[36] V. M. Ustinov, A. Yu. Egorov, A. R. Kovsh, A. E. Zhukov, M. V. Maksimov, A. F. Tsatsul’nikov, N. Y. Gordeev, S. V. Zaitsev, Y. M. Shernyakov, N. A. Bert, P. S. Kop’ev, Zh. I. Alferov, N. N. Ledentsov, J. Böhrer, D. Bimberg, A. O. Kosogov, P. Werner, and U. Gösele,

“Low-threshold injection lasers based on vertically coupled quantum dots, “ *J. Cryst. Growth,* vol. 175-176, no. 2, pp. 689-685, May. 1997.

[37] N. N. Ledentsov, V. A. Shchukin, M. Grundmann, N. Kirstaedter, J. Bo¨hrer, O. Schmidt, D. Bimberg, V. M. Ustinov, A. Yu. Egorov, A. E. Zhukov, P. S. Kop’ev, S. V. Zaitsev, N. Yu. Gordeev, Zh. I. Alferov, A. I. Borovkov, A. O. Kosogov, S. S. Ruvimov, P. Werner, U. Gosele, and J. Heydenreich, “Direct formation of vertically coupled quantum dots in Stranski-Krastanow growth,” *Phys. Rev. B*, vol. 54, no. 12, pp. 8743–8750, Sept. 1996.

[38] A. E. Zhukov, V. M. Ustinov, A. Yu. Egorov, A. R. Kovsh, A. F. Tsatsul’nikov, M. V. Maximov, N. N. Ledentsov, S. V. Zaitsev, N. Y. Gordeev, V. I. Kopchatov, Y. M. Shernyakov, P. S. Kop’ev, D. Bimberg, Zh. I. Alferov, “Injection lasers based on InGaAs quantum dots in an AlGaAs matrix,” *J. Electron. Mater.,* vol. 27, no. 3, pp. 106-109, Mar.
1998.

[39] G. Park, O. B. Shchekin, D. L. Huffaker, and D. G. Deppe, “Low threshold oxide-confined 1.3-μm quantum-dot laser,” *IEEE Photon. Technol. Lett.*, vol. 33, no. 3, pp. 230–232, Mar.
2000.

[40] Y. Wu, “Theory of Modulation Response of Semiconductor Quantum Dot Lasers”, PhD dissertation, Virginia Tech, 2013.

[41] D. Derickson, Fiber optic test and measurement, Prentice-Hall, 1998, p. 642.

[42] D. Bimberg, M. Grundmann and N. N. Ledentsov, Quantum dot heterostructures, John Wiley, 1999, p. 328.

[43] D. L. Huffaker, G. Park, Z. Zou, O. B. Shchekin and D. G. Deppe, "1.3 μm room temperature GaAs-based quantum-dot laser," *Appl. Phys. Lett.*, vol. 73, no. 18, pp. 2564-2566, Nov. 1998.

[44] K. Mukai, Y. Nakata, K. Otsubo, M. Sugawara, N. Yokoyama and H. Ishikawa, "1.3-μm cw lasing of InGaAs-GaAs quantum dots at room temperature with a threshold current of 8 mA," *IEEE Photon. Technol. Lett.*, vol. 11, no. 10, pp. 1205-1207, Oct. 1999.

[45] N. N. Ledentsov, A. R. Kovsh, A. E. Zhukov, N. A. Maleev, S. S. Mikhrin, A. P. Vasil'ev, E. S. Sernenova, M. V. Maximov, Y. M. Shernyakov, N. Kryzhanovskaya, V. Ustinov and D. Bimberg, "High performance quantum dot lasers on GaAs substrates operating in 1.5 μm range," *Electron. Lett.*, vol. 39, no. 15, pp. 1126-1128, Jul. 2003.

[46] H. D. Kim, W. G. Jeong, J. H. Lee, J. S. Yim, D. Lee, R. Stevenson, P. D. Dapkus, J. W. Jang and S. H. Pyun, "Continuous-wave operation of 1.5 μm InGaAs/InGaAsP/InP quantum dot lasers at room temperature," *Appl. Phys. Lett.*, vol. 87, no. 8, Aug. 2005.

[47] L. V. Asryan and R. A. Suris, “Temperature dependence of the threshold current density of a quantum dot laser,” *IEEE. J. Quantum Electron.*, vol. 34, no. 5, pp. 841–850, May. 1998.

[48] L. V. Asryan, R. A. Suris, and S. Luryi, "Internal efficiency of semiconductor lasers with a quantum-confined active region," *IEEE. J. Quantum Electron.*, vol. 39, no. 3, pp. 404–418, Mar. 2003.

[49] P. Bhattacharya, "Quantum well and quantum dot lasers: From strained-layer and self organized epitaxy to high-performance devices," *Optical and Quantum Electron*., vol. 32, no. 3, pp. 211–225, Mar. 2000.

[50] X. Zhang, Y. Yuan, A. Gutierrez-Aitken, and P. Bhattacharya, "GaAs-based multiple quantum well tunneling injection lasers," *Appl. Phys. Lett*., vol. 69, no. 16, pp. 3482–3484, May 2002.

[51] O. B. Shchekin, J. Ahn, D. G. Deppe, "High temperature performance of self-organised quantum dot laser with stacked p-doped active region," *Electron. Lett.,* vol. 38, no.14, pp. 712-713, Jul. 2002.

[52] K. Kamath, D. Klotzkin, and P. Bhattacharya, "Small-signal modulation characteristics of self-organized quantum dot separate confinement heterostructure and tunneling injection lasers," *Proc. IEEE LEOS 10th Annual Meeting*, vol. 2, pp. 498–499, Nov. 1997.

[53] P. Bhattacharya, X. K. Zhang, Y. S. Yuan, K. Kamath, D. Klotzkin, C. Caneau, R. Bhat, "High-speed tunnel injection quantum well and quantum dot lasers," *Proc. SPIE*, vol. 3283, pp. 702–709, Jan. 1998.

[54] P. Bhattacharya and S. Ghosh, "Tunnel injection $In_{0.4}Ga_{0.6}As$/GaAs quantum dot lasers with 15 GHz modulation bandwidth and at room temperature," *Appl. Phys. Lett*., vol. 80, no. 19, pp. 3482–3484, May 2002.

[55] Y. Qiu, D. Uhl, R. Chacon, and R. Q. Yang, "Lasing characteristics of InAs quantum-dot lasers on (001) InP substrate," *Appl. Phys. Lett*., vol. 83, no. 9, pp. 1704–1706, Apr. 2003.

[56] Y. Arakawa, "Fabrication of quantum wires and dots by MOCVD selective growth," *Solid-State Electron*., vol. 37, no. 4–6, pp. 523–528, Apr–Jun. 1994.

[57] L. V. Asryan and S. Luryi, "Tunneling-injection quantum-dot laser: Ultrahigh temperature stability," *IEEE J. Quantum Electron*., vol. 37, no. 7, pp. 905–910, Jul. 2001.

[58] L. V. Asryan and S. Luryi, "Temperature-insensitive semiconductor quantum dot laser," *Solid-State Electron*., vol. 47, no. 2, pp. 205–212, Feb. 2003.

[59] L. V. Asryan and S. Luryi, "Semiconductor laser with reduced temperature sensitivity," *U.S. Patent 6 870 178 B2*, Mar. 22, 2005.

[60] T. Chung, G. Walter, and N. Holonyak, "Coupled strained-layer InGaAs quantum-well improvement of an InAs quantum dot AlGaAs-GaAs-InGaAs-InAs heterostructure laser," *Appl. Phys. Lett*., vol. 79, no. 27, pp. 4500–4502, Dec. 2001.

[61] G. Walter, T. Chung, and N. Holonyak, “High-gain coupled InGaAs quantum well InAs quantum dot AlGaAs-GaAs-InGaAs heterostructure diode laser operation,” *Appl. Phys. Lett.*, vol. 80, no. 7, pp. 1126–1128, Feb. 2002.

[62] G. Walter, T. Chung, and N. Holonyak, “Coupled-stripe quantum-well-assisted AlGaAs-GaAs-InGaAs-InAs quantum-dot laser,” *Appl. Phys. Lett.*, vol. 80, no. 17, pp. 3045–3047, Apr. 2002.

[63] P. K. Kondratko, S.-L. Chuang, G. Walter, T. Chung, and N. Holonyak, “Observations of near-zero linewidth enhancement factor in a quantum-well coupled quantum-dot laser,” *Appl. Phys. Lett.*, vol. 83, no. 23, pp. 4818–4820, Dec. 2003.

[64] L. V. Asryan and R. A. Suris, “Charge Neutrality Violation in Quantum-Dot Laser”, IEEE Journal of Selected Topics in Quantum Electronics, Vol. 3, Number 2, April 1997

[65] L. V. Asryan and Z. N. Sokolova, “Optical power of semiconductor lasers with a low-dimensional active region”, *Journal of Applied Physics*, Vol. 115, issue 2, 023107, Jan 2014

[66] Z. N. Sokolova, I. S. Tarasov and L. V. Asryan, “Threshold characteristics of semiconductor lasers under conditions of violation of electroneutrality in quantum wells”, *Quantum Electronics*, Vol. 43(5), pp 428–432, 2013.

[67] Z. N. Sokolova, N. A. Pikhtin, I. S. Tarasov and L. V. Asryan, “Threshold characteristics of a semiconductor quantum-well laser: inclusion of global electroneutrality in the structure”, *Quantum Electronics*, Vol. 46(9), pp 777–781, 2016

[68] Z. N. Sokolova, D. A. Veselov, N. A. Pikhtin, I. S. Tarasov and L. V. Asryan, “Increase in the internal optical loss with increasing pump current and the output power of quantum well lasers”, *Semiconductors*, Vol. 51(7), 959–964, 2017

[69] E. A. Viktorov, Paul Mandel, “Electron-hole asymmetry and two-state lasing in quantum dot lasers” , Appl. Phys. Lett. 87, 053113 (2005)

[70] Y. Arakawa and A. Yariv, "Quantum well lasers - gain, spectra, dynamics," *IEEE J. Quantum. Electron.*, vol. 22, no. 9, pp. 1887-1899, Sept. 1986.

[71] K. Y. Lau, N. Barchaim, I. Ury, C. Harder and A. Yariv, "Direct amplitude modulation of short-cavity GaAs lasers up to X-band frequencies," *Appl. Phys. Lett.*, vol. 43, no. 1, pp. 1-3, 1983.

[72] K. Uomi, N. Chinone, T. Ohtoshi and T. Kajimura, "High relaxation oscillation frequency (beyond 10 GHz) of GaAlAs multi-quantum well lasers," *Jpn J Appl Phys 2*, vol. 24, no. 7, pp. L539-L541, Jul. 1985.

[73] L. V. Asryan and R. A. Suris, "Upper limit for the modulation bandwidth of a quantum dot

laser," *Appl. Phys. Lett.*, vol. 96, no. 22, Art. no. 221112, May 2010.

[74] K. Kamath, J. Phillips, H. Jiang, J. Singh and P. Bhattacharya, "Small-signal modulation and differential gain of single-mode self-organized $In_{0.4}Ga_{0.6}As$/GaAs quantum dot lasers," *Appl. Phys. Lett.*, vol. 70, no. 22, pp. 2952-2953, Jun. 1997.

[75] S. Fathpour, Z. Mi and P. Bhattacharya, "High-speed quantum dot lasers," *J. Phys. D. Appl. Phys.*, vol. 38, no. 13, pp. 2103-2111, Jul. 2005.

[76] S. Weisser, E. C. Larkins, K. Czotscher, W. Benz, J. Daleiden, I. Esquivias, J. Fleissner, J. D. Ralston, B. Romero, R. E. Sah, A. Schonfelder and J. Rosenzweig, "Damping-limited modulation bandwidths up to 40 GHz in undoped short-cavity In0.35Ga0.65As-GaAs multiple quantum-well lasers," *IEEE Photon. Technol. Lett.*, vol. 8, no. 5, pp. 608-610, May 1996.

Chapter 2

Effect of Out-Tunneling Leakage on Modulation Bandwidth in Double Tunneling-Injection Quantum Dot Lasers

Summary

The effect of out-tunneling leakage of carriers from QDs in limiting the modulation bandwidth of a DTI QD laser was analyzed. To purely focus on this effect, the conditions of instantaneous carrier exchange between the OCL and QW (on each side of the structure) and tunneling injection into QDs are assumed. The relative decrease in modulation bandwidth in DTI QD laser is then shown to be small, and at ranges of injection currents of operational interest, nearly negligible. Consequently, it was shown that the DTI laser is a robust device in terms of sensitivity to out-tunneling leakage i.e. much effort need not be paid in suppressing this phenomenon.

2.1. Introduction

In order to improve on the various drawbacks of "conventional" QD lasers[1-21], tunneling-injection quantum dot lasers[22-29], and since then double tunneling-injection Quantum Dot (DTI QD) lasers[30-32] have been proposed.

Briefly, the "conventional" QD laser suffers as it fails to take into account that a large fraction of the injection current will be wasted in electron-hole recombinations in the reservoir[11]. Additionally, temperature dependence of the threshold current occurs due to parasitic recombination outside the QD's[12]. In [13] it was shown that the carrier capture delay in conventional QD lasers is also responsible for low modulation bandwidth.

The DTI QD laser design addresses all these concerns. By controlling parasitic recombination, it has been shown that the characteristic temperature $\boldsymbol{T_o}$ can theoretically be made to be in of 1000 K (in DTI lasers) [30]-[32]. In DTI lasers, direct tunneling of both electrons and holes should leads to effective and fast pumping of lasing states in QDs. Hence, a high direct modulation bandwidth is to be expected. Although the DTI design is challenging to fabricate, initial experimental studies [33]-[36] have already shown improvements in gain[34] and symmetrical gain shape and a smaller refractive index change at the peak gain wavelength [36]. Hence, we believe that the DTI QD laser design must be investigated further.

In real world operations, out-tunneling leakage always occurs and to truly test the effectiveness of the DTI QD laser design, its effect on the modulation bandwidth must also be explored in order to estimate the true performance of such a device.

2.2. Theoretical model

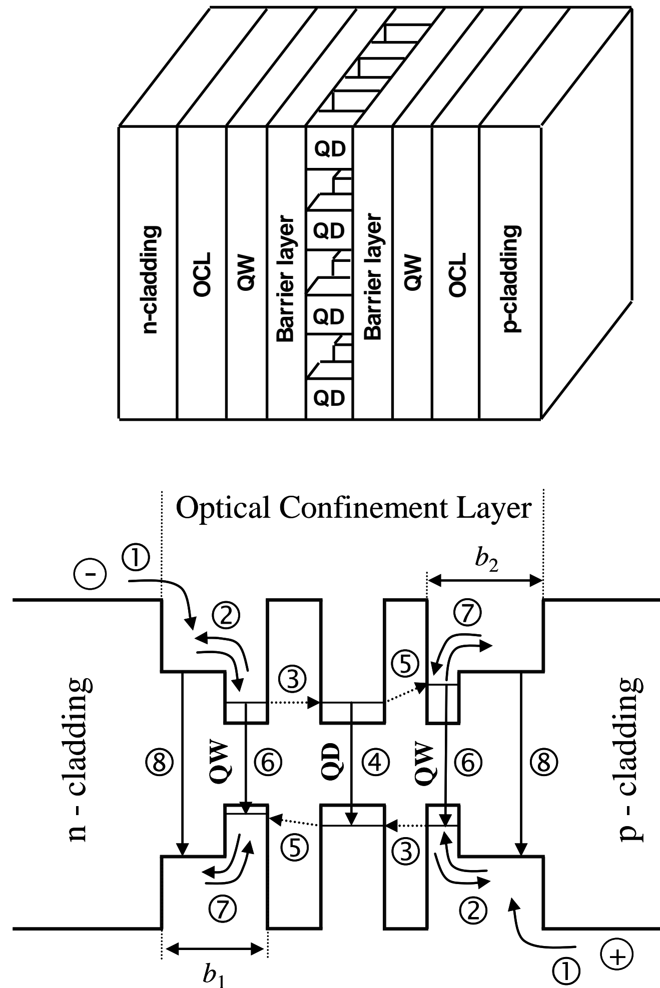

Fig. 2.1. Schematic side view and energy band diagram of a double tunneling-injection (DTI) QD laser. (Reprinted with permission from fig. 1 of [30] © 2011 IEEE)

In the fig. shown [fig.2.1.], the QWs and the QDs are assumed implemented in the same material, although this does not have to be necessarily the case in general. The electron-injecting QW is wider than the hole-injecting QW and both QWs are narrower than the QD to accomplish resonant alignment of the majority-carrier subbands with the QD energy levels. The tunnel barrier on the electron-injecting side is made thicker to suppress out-tunneling leakage of holes from the QD.

The main processes are labeled as follows:

"1". Injection from the cladding layers to the OCL.

"2". Majority carrier capture from the OCL to the QW and thermal escape from the QW to the OCL.

"3". Tunneling-injection from the QW into a QD.

"4". Spontaneous and stimulated recombination in a QD.

"5". Out-tunneling from a QD into the "foreign" QW.

"6". Spontaneous recombination in the QWs.

"7". Minority carrier thermal escape from the QW to the OCL and capture from the OCL to the QW, and

"8". Spontaneous recombination in the OCL.

2.2.1. Main assumptions

Let us first focus on one of the factors, which can limit the modulation bandwidth of a DTI QD laser, – the out-tunneling leakage of carriers from QDs. In properly designed structures, out-tunneling processes can be effectively suppressed. In un-optimized structures, these processes can however occur with a non-zero rate. Here $w^{R}_{\mathrm{n,\,tunn}}$ and $w^{L}_{\mathrm{p,\,tunn}}$ are non-zero and hence the tunneling times of electrons from a QD to the hole-injecting QW [see eq. (18)] and holes from a QD to the electron-injecting QW are finite. To first purely focus on the effect of out-tunneling leakage, we will make the following assumptions:

- Carrier exchange between the OCL and QW on each side of the structure is instantaneous ($\mathrm{v}^{L,R}_{\mathrm{n,p,capt}} \to \infty$ and $\tau^{L,R}_{\mathrm{n,p,esc}} \to 0$).
- Tunneling-injection into QDs (processes "3" in Fig. 1) is instantaneous ($w^{L}_{\mathrm{n,\,tunn}} \to \infty$ and $w^{R}_{\mathrm{p,\,tunn}} \to \infty$).

We will calculate the modulation bandwidth as a function of the out-tunneling coefficients $w^{R}_{\mathrm{n,\,tunn}}$ and $w^{L}_{\mathrm{p,\,tunn}}$, i.e., the out-tunneling times from a QD to the "foreign" QWs. The equations listed below have been numerically solved using Mathcad 5.

For further analysis of equations, refer to Appendix A.

2.2.2. Rate equations

We have the following set of three rate equations for finding f_n, F_{QW}, and n_{ph}:

$$\frac{\partial}{\partial t}\left[\left(\frac{b_1 n_1}{N_c^{2D}}+1\right)N_c^{2D}\frac{f_n}{1-f_n}+2N_S f_n\right]=\frac{j}{e}-\left[\frac{b_1 B n_1^2}{(N_c^{2D})^2}+B_{2D}\right]N_c^{2D}\frac{f_n}{1-f_n}F_{QW} \\ -N_S\frac{f_n^2}{\tau_{QD}}-[w_{out-tunn}F_1^{QW}N_S f_n-w_{out-tunn}N_S(1-f_n)F_{QW}]-v_g g^{max}(2f_n-1)n_{ph} \quad , \quad (2.1)$$

$$\frac{\partial}{\partial t}\left[\left(\frac{b_1 n_1}{N_c^{2D}}+1\right)F_{QW}\right]=[w_{out-tunn}F_1^{QW}N_S f_n-w_{out-tunn}N_S(1-f_n)F_{QW}] \\ -\left[\frac{b_1 B n_1^2}{(N_c^{2D})^2}+B_{2D}\right]N_c^{2D}\frac{f_n}{1-f_n}F_{QW} \quad , \quad (2.2)$$

$$\frac{\partial n_{ph}}{\partial t}=v_g g^{max}(2f_n-1)n_{ph}-v_g\beta n_{ph} \quad (2.3)$$

where

b_1 thickness of the OCL.

F_1^{QW} in case of an undoped QW and a resonance between the energy level in a QD and the lowest sub-band edge in a QW, is the 2-D effective densities of states in the conduction and valence bands in the QWs. (Refer to eqn. 25 of Appendix A).

F_{QW} minority carrier densities in the foreign QWs.

B , B_{2D} spontaneous radiative recombination constants for the bulk (OCL) and 2-D regions (QWs) measured in units of cm^3/s and cm^2/s, respectively.

N_S surface density of QDs.

f_n electron (and hole) level occupancies in QDs with

τ_{QD} spontaneous radiative lifetime in QD.

v_g group velocity of light,

g^{max} maximum value of the modal gain

n_{ph} 2-D density of photons in the lasing mode (number of photons per unit area of the junction).

N_c^{2D} 2-D effective densities of states in the conduction (and valence band) in the QWs.

n_1 (3-D) effective densities of states in conduction and valence bands in the OCL.

w_{out} coefficient for electron and hole out-tunneling between QD ensemble and QWs.

2.2.3 Small-signal analysis

On applying small-signal analysis to rate equations (2.1)-(2.3) we consider the injection current density in (2.1) in the form of

$$j = j_0 + (\delta j_{\mathrm{m}}) \exp(i\omega t)\,, \tag{2.4}$$

where j_0 is the dc component and the amplitude δj_{m} of the time-harmonic ac component is small ($\delta j_{\mathrm{m}} << j_0 - j_{\mathrm{th}}$, where j_{th} is the threshold current density). We will correspondingly look for f_{n}, F_{QW}, and n_{ph} in (1)-(3) in the form of

$$F_{\mathrm{QW}} = F_{\mathrm{QW,0}} + (\delta F_{\mathrm{QW-m}}) \exp(i\omega t)\,, \tag{2.5}$$

$$f_{\mathrm{n}} = f_{\mathrm{n,0}} + (\delta f_{\mathrm{n-m}}) \exp(i\omega t)\,, \tag{2.6}$$

$$n_{\mathrm{ph}} = n_{\mathrm{ph,0}} + (\delta n_{\mathrm{ph-m}}) \exp(i\omega t)\,, \tag{2.7}$$

where the dc components $f_{\mathrm{n,0}}$, $F_{\mathrm{QW,0}}$, and $n_{\mathrm{ph,0}}$ are the solutions of rate equations (2.1)-(2.3) at the steady-state ($\partial/\partial t = 0$ in the left-hand side of these equations), which correspond to the dc component j_0 of the injection current density.

Using (2.4)-(2.7) in (2.1)-(2.3), we will obtain a set of linear algebraic equations in the frequency-dependent small amplitudes $\delta f_{\mathrm{n-m}}$, $\delta F_{\mathrm{QW-m}}$, and $\delta n_{\mathrm{ph-m}}$. The solution of this algebraic set will yield the modulation response function which is defined as,

$$H(\omega) = \left| \frac{\delta n_{\mathrm{ph-m}}(\omega)}{\delta n_{\mathrm{ph-m}}(0)} \right|^2 . \tag{2.8}$$

Using eq(A2.54) for $\delta n_{\mathrm{ph-m}}(i\omega)/\delta n_{\mathrm{ph-m}}(0)$ (see Appendix C) for the response function, we have,

$$H(\omega) = \frac{C_{13}{}^2 C_{31}{}^2 D_{22}{}^2}{\left[C_{13}C_{31}D_{22} + \omega^2 (Y_1 D_{22} + Y_2 D_{11})\right]^2 + \omega^2 \left[\left(Y_2 C_{13} C_{31} + C_{12} C_{21} - D_{11} D_{22}\right) + \omega^2 Y_1 Y_2\right]^2}\,, \tag{2.9}$$

where the coefficients C_{ij}, D_{ij} and Y_i are given in Appendix C

Having $H(\omega)$, we will calculate the modulation bandwidth, which is defined as the –3 dB bandwidth [the frequency at which the response function $H(\omega)$ has fallen to half its dc ($\omega = 0$) value],

$$10\log_{10} H(\omega_{-3\,\mathrm{dB}}) = -3 \tag{2.10}$$

For ω_{-3db} we obtain the following cubic equation in $\omega^2_{-3\mathrm{dB}}$,

$$\omega^6_{-3\mathrm{dB}} + E_4\omega^4_{-3\mathrm{dB}} + E_2\omega^2_{-3\mathrm{dB}} - E_0 = 0 \tag{2.11}$$

where the coefficients E_0, E_2 and E_4 are given in the Appendix C.

2.3. Discussion

Modulation bandwidth vs injection current density (*j₀*)

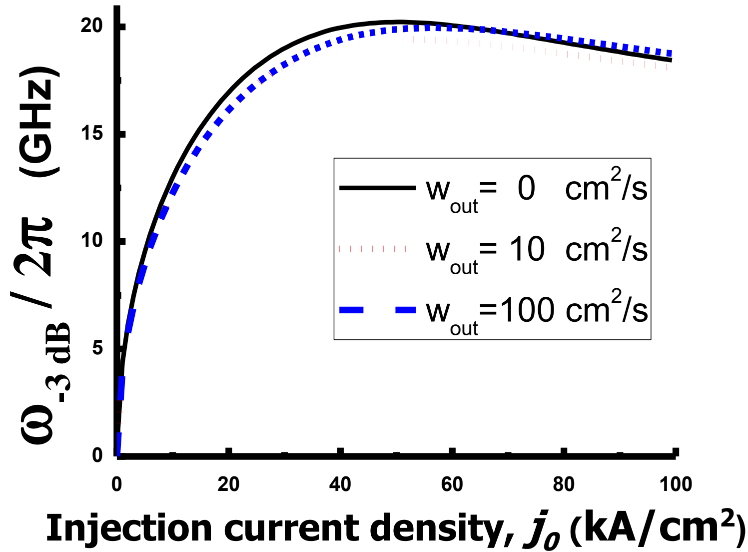

Fig. 2.2. Modulation bandwidth vs Injection current density (j_0) for various out-tunneling coefficients. The other parameters (kept constant) here are: Tunneling offset energy (Δ) = $2k_bT$, N_s =6.109 x 10^{10} cm^{-2}, Cavity length L = 0.114 cm ,Inhomogeneous line broadening (δ) = 0.05

In order to investigate the effect of out-tunneling, our first task was to calculate the modulation bandwidth ($\omega_{-3\mathrm{dB}}$) at different out-tunneling coefficients for all injection currents greater than the threshold current (i.e. the current at which gain is equal to loss and above which lasing starts). On increasing the injection current density (above the threshold current density), we

see [fig. 2.2.] the modulation bandwidth $\omega_{-3\mathrm{dB}}$ increases from zero (as at threshold current lasing starts), approaches a maximum and then decreases. This general trend holds for all values of out-tunneling. There are some very interesting things to note however. Firstly, for higher out-tunneling coefficients, modulation bandwidth approaches a constant value. Moreover, this value of $\omega_{-3\mathrm{dB}}$ is relatively high.

Secondly, the fact that the curves for various out-tunneling coefficients almost coincide with each other. This would indicate that very little variation in modulation bandwidth occurs on increasing the out-tunneling coefficient.

Modulation bandwidth vs out-tunneling coefficient (w_{out}) and off–resonance energy (Δ)

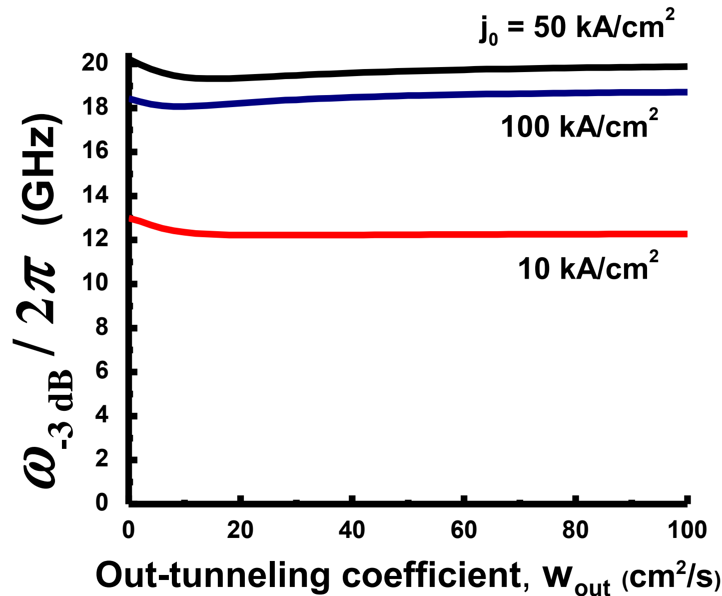

Fig. 2.3. Modulation bandwidth vs out-tunneling coefficient (w_{out}) for various injection current densities. The other parameters (kept constant) here are: Tunneling offset energy (Δ) = $2k_bT$, N_s =6.109 x 10^{10} cm^{-2}, Cavity length L = 0.114 cm ,Inhomogeneous line broadening (δ) = 0.05

Furthermore, to analyze whether this low relative change in modulation bandwidth with increase in out-tunneling leakage holds at all values of the out-tunneling coefficient we plot the curve of $\omega_{-3\mathrm{dB}}$ versus the out-tunneling coefficient for various values of injection current density j_0.

From fig. 2.3. , we see that the general trend, is that $\omega_{-3\text{dB}}$ decreases initially to a point of minima and then increases asymptotically, confirming our previous finding that $\omega_{-3\text{dB}}$ saturates with higher out-tunneling.

The question now arises as to why the effect of out-tunneling isn't more pronounced. The out-tunneling flux is given in equation (13) as $w^{R}_{n,tunn} .n_1^{R,QW} .N_\text{S} .f_n$. Here $\boldsymbol{w^{R}_{n,tunn}}$, $\boldsymbol{n_1^{R,QW}}$ and $\boldsymbol{N_\text{s}}$ are constants and stand for the out-tunneling coefficient to the right (hole injecting) QW, the equilibrium carrier concentration in the right QW, and the two dimensional surface density of QDs respectively. The only variable here is the probability of occupation $\boldsymbol{f_n}$ whose maximum value is limited to unity. Hence, we can see that even in the worst possible scenario, the impact of this term is inherently limited. As a result the variation of the modulation bandwidth seen is small.

We see that for various injection currents, increasing the out-tunneling coefficient does result in an overall lowering of the modulation bandwidth for a given injection current density, however the relative drop at relevant levels of injection current is negligible. Moreover, for higher out-tunneling coefficients, we see that the modulation bandwidth saturates. This indicates that such device, in terms of out-tunneling is highly robust.

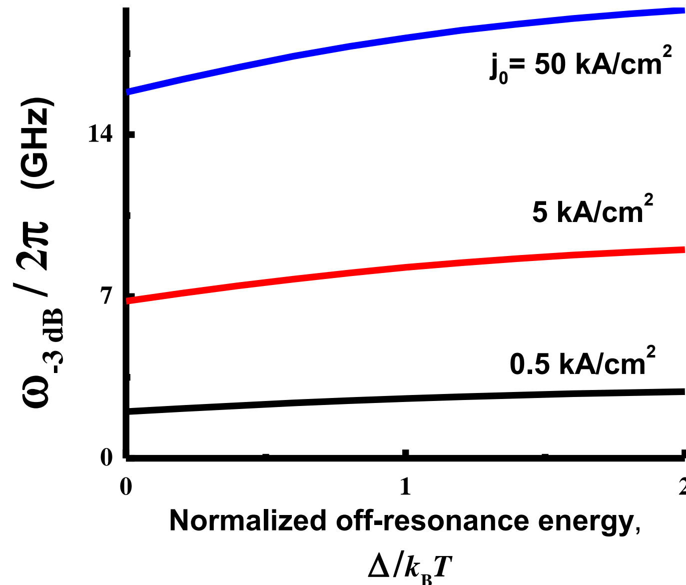

Fig. 2.4. Modulation bandwidth vs off–resonance energy (*Δ*) for various injection current densities. The other parameters here are: Out-tunneling coefficient (w_{out}) = 10 cm^2/s , N_s =6.109 x 10^{10} cm^{-2}, Cavity length *L* = 0.114 cm, Inhomogeneous line broadening (δ) = 0.05

Our next objective was to analyze the effect of off-resonance energy of out-tunneling on the modulation bandwidth. Tunneling offset energy (Δ) is the difference (off-resonance) in energy [fig. 2.5.] between the energy of the electron level in the QD and the electron level in the "foreign" QW.

For this we plotted modulation bandwidth as a function of the (normalized) off-resonance energy for various values of injection current density [fig. 2.4.]. The first conclusion we draw is that on increasing the off-resonance energy, modulation bandwidth increases. This, of course is a natural outcome and is to be expected. On increasing the off-resonance energy, we are reducing the probability of electrons and holes to tunnel out and escape. Consequently, the modulation bandwidth increases due to less leakage. More importantly, we see that the plotted lines are fairly flat. This goes on to indicate that the relative drop in modulation bandwidth due to decreasing off-resonance energy is low. This is then further analyzed in fig. 2.6.

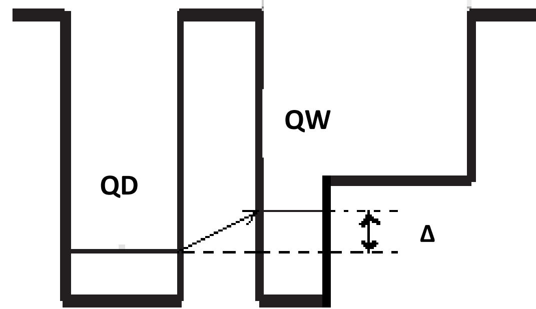

Fig. 2.5. Schematic depicting off–resonance energy (*Δ*) for a DTI QD laser

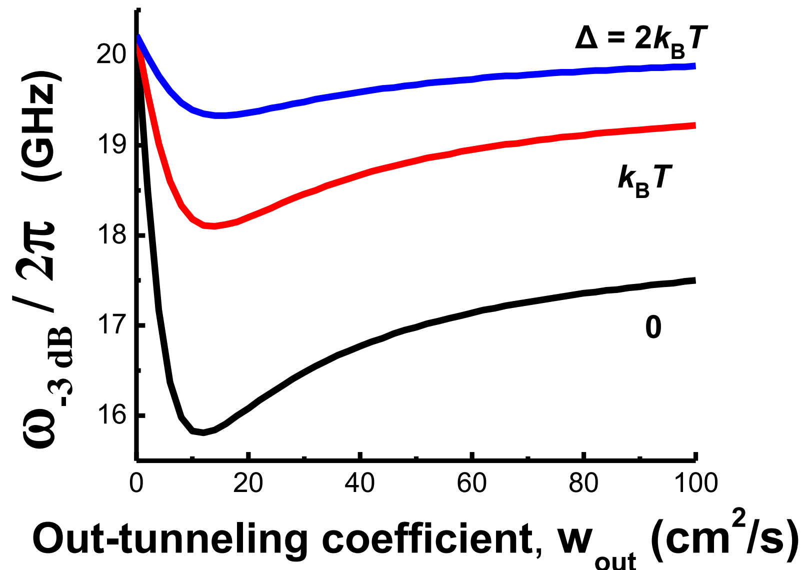

Fig. 2.6. Modulation bandwidth vs out-tunneling coefficient (w_{out}) for various off–resonance energies (*Δ*). The other parameters here are: Injection current density (j_0) = 50 kA/cm^2, N_s =6.109 x 10^{10} cm^{-2}, Cavity length L = 0.114 cm, Inhomogeneous line broadening (δ) = 0.05

In fig 2.6., again we see that on increasing the off-resonance energy, modulation bandwidth increases. The point of interest however is that even in case of off-resonance energy ($\varDelta$) = 0, corresponding to resonant out-tunneling between the QD and the "foreign" QW, the relative drop in modulation bandwidth remains low i.e. even in ***the worst case scenario*****,** the **relative drop in modulation bandwidth remains low**.

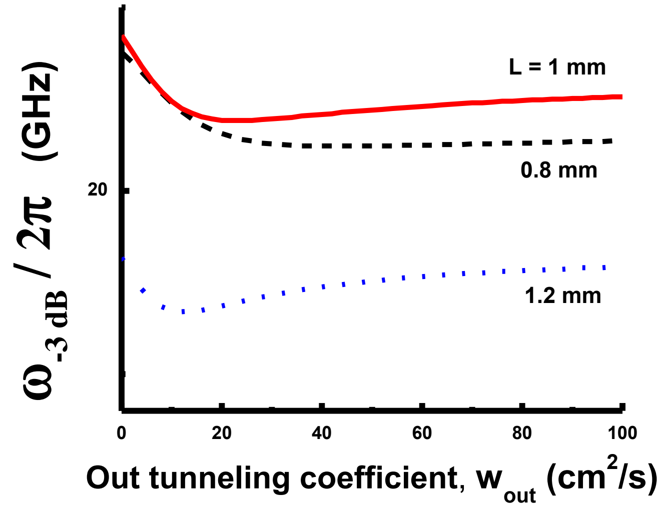

Fig. 2.7. Modulation bandwidth vs out-tunneling coefficient (w_{out}) for various cavity lengths (L). The other parameters here are: Injection current density (j_0) = 50 kA/cm^2, N_s =6.109 x 10^{10} cm^{-2}, Tunneling offset energy ($\varDelta$) = $2k_bT$, Inhomogeneous line broadening (δ) = 0.05

We found some interesting results about the effect of out-tunneling on the modulation bandwidth, but for these conclusions to hold we must analyze the effect of both QD surface density (N_s) and cavity length (L) on out-tunneling. For both these parameters, we see similar trends. We do see that at minimum (threshold) values of both ***Ns*** and ***L*** [fig. 2.7. and fig. 2.8.] the modulation bandwidth is fairly low, but this is owing to the fact that near these threshold values the modulation bandwidth is already low.

For more practical values, relative drop in bandwidth is again not significant. Curve nature also remains the same, decreasing first to reach a minima and then tending to increase to a steady value for higher out-tunneling coefficients. From [37] we already know that for both ***Ns*** and ***L*** modulation bandwidth does not continuously increase, but rather reaches a maximum and then decrease on further increase. An interesting phenomena is that the final decrease is sharper for ***L*** than ***Ns*** [fig. 2.9.].

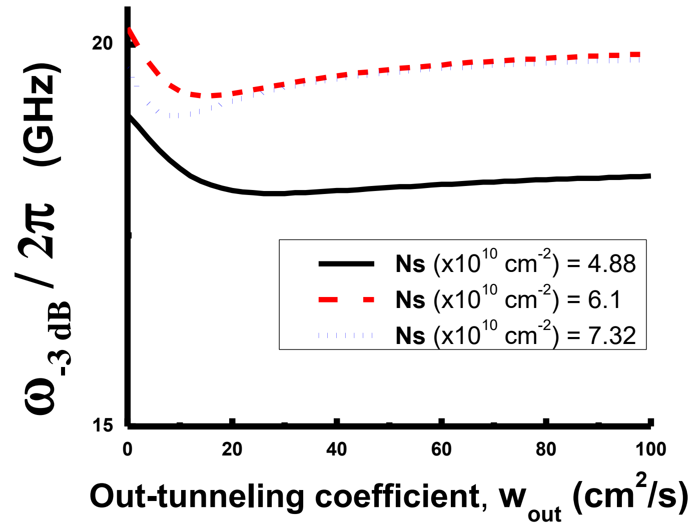

Fig. 2.8. Modulation bandwidth vs out-tunneling coefficient (w_{out}) for various QD surface densities (Ns). The other parameters here are: Injection current density (j_0) = 50 kA/cm², Cavity length L = 0.114 cm, Tunneling offset energy (Δ) = $2k_bT$, Inhomogeneous line broadening (δ) = 0.05

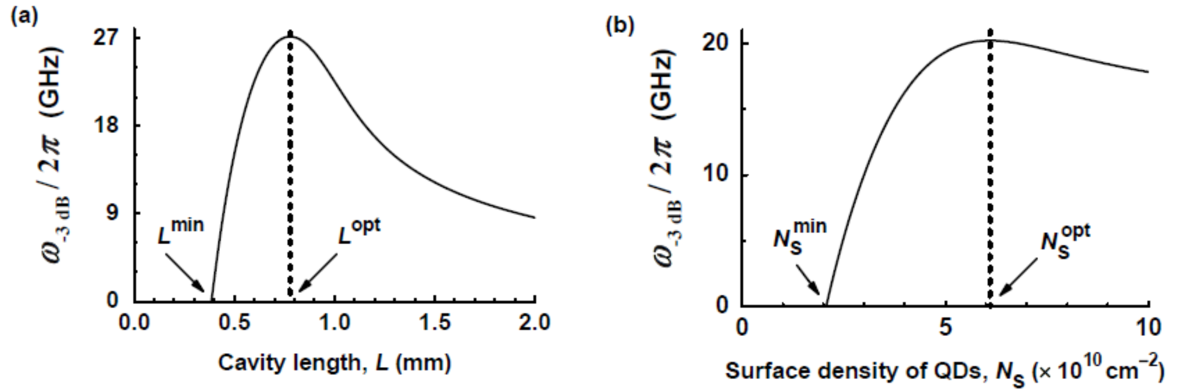

Fig. 2.9. Modulation bandwidth vs cavity length and QD surface density in an ideal double tunneling-injection quantum dot laser. (Reprinted with permission from fig. 5 of [37])

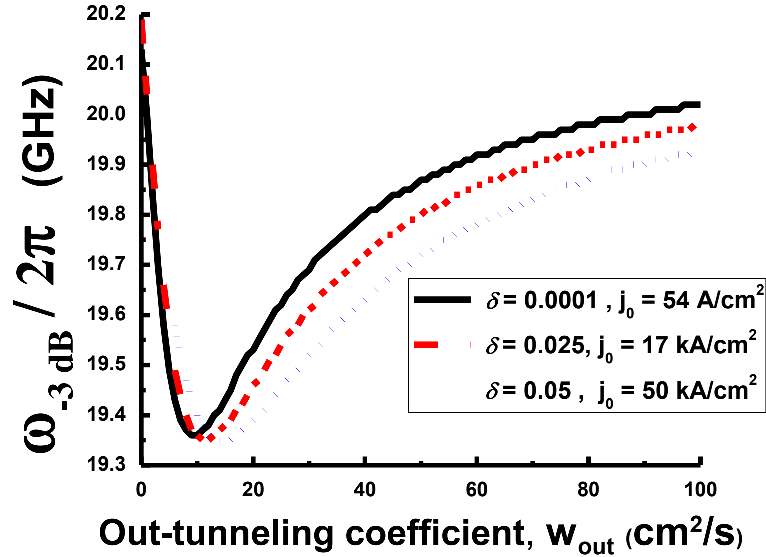

Fig. 2.10. Modulation bandwidth vs out-tunneling coefficient (w_{out}) for various values of line broadening (δ). The other parameters here are: Cavity length L = 0.114 cm, Tunneling offset energy (Δ) = $2k_bT$, N_s =6.109 x 10^{10} cm^{-2}

In fig 2.10., it was shown that at realistic values of line broadening, relative drop in modulation bandwidth is low. It can be noted that the current density is different for each of the curves. This is because on changing the line broadening, the optimum current injection density changes. The curves for $\boldsymbol{\delta}$ were then plotted at the corresponding optimum current densities. On lowering line broadening and then plotting against the out-tunneling coefficient, maximum modulation bandwidth remains relatively unaffected as the curves remain close to each other.

2.4. Conclusion

On analyzing the effect of out-tunneling leakage of carriers from QDs in limiting the modulation bandwidth of a DTI QD laser, we are confronted with results of significant relevance. It can be noted from the very outset (plots of modulation bandwidth vs j on increasing w_{out}) that there is low relative reduction in modulation bandwidth i.e. out-tunneling does not sufficiently reduce the effectiveness of such a DTI design. Further, for higher out-tunneling coefficients, the relative drop in modulation bandwidth saturates and approaches a constant value. We then find that even for the worst case scenario i.e. in the case of resonant out-tunneling, relative reduction in modulation bandwidth remains low.

We go on to check that for various values of tunneling offset energy (Δ), surface densities of QDs (**Ns**),cavity lengths (**L**) and line broadening (Δ) the nature of the above result does not change, where for these values being within operational ranges, modulation bandwidth remains sufficiently large.

From this, we draw a reasonable and commercially significant conclusion, that the DTI QD laser is a fairly robust device in terms of sensitivity to out-tunneling leakage i.e. much effort need not be paid in suppressing this phenomenon.

Appendix A: Analysis of Rate Equations

Our model is based on the following set of rate equations, which include the main processes in the layered structure (Fig.2.1.). These equations have then been numerically evaluated using Mathcad.

for free electrons and holes in the left-hand side of the OCL,

$$b_1 \frac{\partial n_L}{\partial t} = \frac{j}{e} + \frac{n_{\mathrm{QW}}^L}{\tau_{\mathrm{n,esc}}^L} - \mathrm{v}_{\mathrm{n,capt}}^L n_L - b_1 B n_L p_L \,, \tag{A2.1}$$

$$b_1 \frac{\partial p_L}{\partial t} = \frac{p_{\mathrm{QW}}^L}{\tau_{\mathrm{p,esc}}^L} - \mathrm{v}_{\mathrm{p,capt}}^L p_L - b_1 B n_L p_L \,, \tag{A2.2}$$

for free holes and electrons in the right-hand side of the OCL,

$$b_2 \frac{\partial p_R}{\partial t} = \frac{j}{e} + \frac{p_{\mathrm{QW}}^R}{\tau_{\mathrm{p,esc}}^R} - \mathrm{v}_{\mathrm{p,capt}}^R p_R - b_2 B n_R p_R \,, \tag{A2.3}$$

$$b_2 \frac{\partial n_R}{\partial t} = \frac{n_{\mathrm{QW}}^R}{\tau_{\mathrm{n,esc}}^R} - \mathrm{v}_{\mathrm{n,capt}}^R n_R - b_2 B n_R p_R \,, \tag{A2.4}$$

for electrons and holes in the electron-injecting (left-hand-side) QW,

$$\frac{\partial n_{\mathrm{QW}}^L}{\partial t} = \mathrm{v}_{\mathrm{n,capt}}^L n_L - \frac{n_{\mathrm{QW}}^L}{\tau_{\mathrm{n,esc}}^L} - w_{\mathrm{n,\,tunn}}^L N_S (1 - f_{\mathrm{n}}) n_{\mathrm{QW}}^L + w_{\mathrm{n,tunn}}^L n_1^{L,\mathrm{QW}} N_S f_{\mathrm{n}} - B_{\mathrm{2D}} n_{\mathrm{QW}}^L p_{\mathrm{QW}}^L \,, \tag{A2.5}$$

$$\frac{\partial p_{\mathrm{QW}}^L}{\partial t} = \mathrm{v}_{\mathrm{p,capt}}^L p_L - \frac{p_{\mathrm{QW}}^L}{\tau_{\mathrm{p,esc}}^L} - w_{\mathrm{p,tunn}}^L N_S (1 - f_{\mathrm{p}}) p_{\mathrm{QW}}^L + w_{\mathrm{p,tunn}}^L p_1^{L,\mathrm{QW}} N_S f_{\mathrm{p}} - B_{\mathrm{2D}} n_{\mathrm{QW}}^L p_{\mathrm{QW}}^L \,, \tag{A2.6}$$

for holes and electrons in the hole-injecting (right-hand-side) QW,

$$\frac{\partial p_{\mathrm{QW}}^R}{\partial t} = \mathrm{v}_{\mathrm{p,capt}}^R p_R - \frac{p_{\mathrm{QW}}^R}{\tau_{\mathrm{p,esc}}^R} - w_{\mathrm{p,tunn}}^R N_S (1 - f_{\mathrm{p}}) p_{\mathrm{QW}}^R + w_{\mathrm{p,tunn}}^R p_1^{R,\mathrm{QW}} N_S f_{\mathrm{p}} - B_{\mathrm{2D}} n_{\mathrm{QW}}^R p_{\mathrm{QW}}^R \,, \tag{A2.7}$$

$$\frac{\partial n_{\mathrm{QW}}^R}{\partial t} = \mathrm{v}_{\mathrm{n,capt}}^R n_R - \frac{n_{\mathrm{QW}}^R}{\tau_{\mathrm{n,esc}}^R} - w_{\mathrm{n,tunn}}^R N_S (1 - f_{\mathrm{n}}) n_{\mathrm{QW}}^R + w_{\mathrm{n,tunn}}^R n_1^{R,\mathrm{QW}} N_S f_{\mathrm{n}} - B_{\mathrm{2D}} n_{\mathrm{QW}}^R p_{\mathrm{QW}}^R \,, \tag{A2.8}$$

for electrons and holes confined in QDs,

$$2N_S \frac{\partial f_{\mathrm{n}}}{\partial t} = w_{\mathrm{n,tunn}}^L N_S (1 - f_{\mathrm{n}}) n_{\mathrm{QW}}^L - w_{\mathrm{n,tunn}}^L n_1^{L,\mathrm{QW}} N_S f_{\mathrm{n}} + w_{\mathrm{n,tunn}}^R N_S (1 - f_{\mathrm{n}}) n_{\mathrm{QW}}^R - w_{\mathrm{n,tunn}}^R n_1^{R,\mathrm{QW}} N_S f_{\mathrm{n}} - N_S \frac{f_{\mathrm{n}} f_{\mathrm{p}}}{\tau_{\mathrm{QD}}} - \mathrm{v}_{\mathrm{g}} g^{\max} (f_{\mathrm{n}} + f_{\mathrm{p}} - 1) n_{\mathrm{ph}} \,, \tag{A2.9}$$

$$2N_S \frac{\partial f_{\rm p}}{\partial t} = w_{\rm p,tunn}^R N_S (1-f_{\rm p}) p_{\rm QW}^R - w_{\rm p,tunn}^R p_1^{R,\rm QW} N_S f_{\rm p} + w_{\rm p,tunn}^L N_S (1-f_{\rm p}) p_{\rm QW}^L - w_{\rm p,tunn}^L p_1^{L,\rm QW} N_S f_{\rm p}$$
$$- N_S \frac{f_{\rm n} f_{\rm p}}{\tau_{\rm QD}} - {\rm v}_{\rm g} g^{\max} (f_{\rm n} + f_{\rm p} - 1) n_{\rm ph}, \tag{A2.10}$$

and for photons,

$$\frac{\partial n_{\rm ph}}{\partial t} = {\rm v}_{\rm g} g^{\max} (f_{\rm n} + f_{\rm p} - 1) n_{\rm ph} - {\rm v}_{\rm g} \beta n_{\rm ph}\,. \tag{A2.11}$$

In eqs. (A2.1)–(A2.11), b_1 (b_2) is the thickness of the left- (right-) hand side of the OCL [the separation between the *n*- (*p*-) cladding layer and the left- (right-) hand-side barrier – Fig. 2.1] and n_L (n_R) and p_L (p_R) are the free-electron and -hole densities there, j is the injection current density, e is the electron charge, $n_{\rm QW}^L$ ($n_{\rm QW}^R$) and $p_{\rm QW}^L$ ($p_{\rm QW}^R$) are the 2-D electron and hole densities in the left- (right-) hand-side QW (Fig. 2.1), B and $B_{\rm 2D}$ are the spontaneous radiative recombination constants for the bulk (OCL) and 2-D regions (QWs) measured in units of cm^3/s and cm^2/s, respectively, N_S is the surface density of QDs, $f_{\rm n,p}$ are the electron- and hole-level occupancies in QDs, $\tau_{\rm QD}$ is the spontaneous radiative lifetime in QDs, ${\rm v_g}$ is the group velocity of light, $g^{\max}$ is the maximum value of the modal gain [11], $\beta = (1/L)\ln(1/R)$ is the mirror loss, L is the cavity length, R is the facet reflectivity, and $n_{\rm ph}$ is the 2-D density of photons in the lasing mode (number of photons per unit area of the junction).

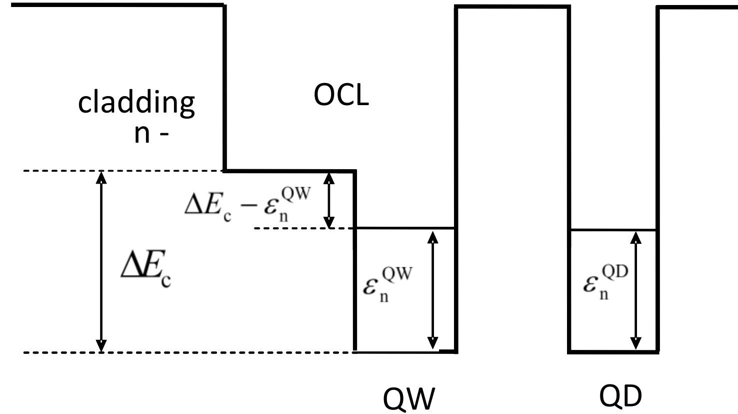

Fig. 2.11. Conduction band diagram in the left-hand (electron-injecting) side of the structure.

We denoted the thermal escape times of electrons and holes from the QWs to the OCL by $\tau_{\rm n,p,esc}^{L,R}$ and the capture velocities from the OCL to the QWs by ${\rm v}_{\rm n,p,capt}^{L,R}$. These quantities are related to each other. It is the capture velocity (measured in units of cm/s) that genuinely describes the carrier capture to a QW [38, 39, 40]. For undoped OCL and QW, the relation between $\tau_{\rm n,p,esc}$ and ${\rm v}_{\rm n,p,capt}$ reads as follows:

$$\tau_{\mathrm{n,esc}} = \frac{1}{\mathrm{v}_{\mathrm{n,capt}}} \frac{N_{\mathrm{c}}^{\mathrm{2D}}}{n_1}, \qquad \tau_{\mathrm{p,esc}} = \frac{1}{\mathrm{v}_{\mathrm{p,capt}}} \frac{N_{\mathrm{v}}^{\mathrm{2D}}}{p_1}, \tag{A2.12}$$

where

$$N_{\mathrm{c,v}}^{\mathrm{2D}} = \frac{m_{\mathrm{c,v}}^{\mathrm{QW}} T}{\pi \hbar^2} \tag{A2.13}$$

are the 2-D effective densities of states in the conduction and valence bands in the QWs, $m_{\mathrm{c,v}}^{\mathrm{QW}}$ are the electron and hole effective masses in the QWs, and the temperature T is measured in units of energy.

The quantities n_1 and p_1 are

$$n_1 = N_{\mathrm{c}}^{\mathrm{3D}} \exp\left(-\frac{\Delta E_{\mathrm{c}} - \varepsilon_{\mathrm{n}}^{\mathrm{QW}}}{T}\right), \qquad p_1 = N_{\mathrm{v}}^{\mathrm{3D}} \exp\left(-\frac{\Delta E_{\mathrm{v}} - \varepsilon_{\mathrm{p}}^{\mathrm{QW}}}{T}\right), \tag{A2.14}$$

where

$$N_{\mathrm{c,v}}^{\mathrm{3D}} = 2\left(\frac{m_{\mathrm{c,v}}^{\mathrm{OCL}} T}{2\pi \hbar^2}\right)^{3/2} \tag{A2.15}$$

are the three-dimensional (3-D) effective densities of states in the conduction and valence bands in the OCL, $m_{\mathrm{c,v}}^{\mathrm{OCL}}$ are the electron and hole effective masses in the OCL, $\Delta E_{\mathrm{c,v}}$ are the conduction and valence band offsets between the OCL and the QW (Fig. 2.11), and $\varepsilon_{\mathrm{n,p}}^{\mathrm{QW}}$ are the energies of the lowest electron- and hole-subband edges in the QW (Fig. 2.11).

We exploit four tunneling coefficients, $w_{\mathrm{n,p,\,tunn}}^{L,R}$ (measured in units of cm^2/s), for electron and hole tunneling between the QD ensemble and the QWs. These tunneling coefficients are primarily controlled by the thicknesses and material parameters of the barriers, and by the QD and QW parameters as well. In a properly designed structure, $w_{\mathrm{n,\,tunn}}^{L}$ and $w_{\mathrm{p,\,tunn}}^{R}$ should be large, and $w_{\mathrm{p,\,tunn}}^{L}$ and $w_{\mathrm{n,\,tunn}}^{R}$ small.

The quantities $n_1^{L,R,\mathrm{QW}}$ and $p_1^{L,R,\mathrm{QW}}$ entering into the electron and hole tunneling fluxes from the QD ensemble to the QWs [see (A2.5)–(A2.10)] are measured in units of cm^{-2}. In the case of an undoped QW and a resonance between the energy level in a QD and the lowest sub-band edge in a QW, the expressions for n_1^{QW} and p_1^{QW} are

$$n_1^{L,\mathrm{QW}} = N_{\mathrm{c}}^{\mathrm{2D}}, \qquad p_1^{R,\mathrm{QW}} = N_{\mathrm{v}}^{\mathrm{2D}}. \tag{A2.16}$$

As seen from (A2.1)–(A2.8), the equations for the carrier densities in the right-hand-side QW and OCL are similar to those in the left-hand side. For this reason, we describe below the terms entering the equations for the carrier densities in the left-hand side of the structure only.

The first term in the right-hand side in eq. (A2.1) is the electron injection flux (in units of $\text{cm}^{-2}\text{s}^{-1}$) from the n-cladding layer to the OCL.

The terms containing the escape times and capture velocities in the rate equations are respectively the fluxes of thermal escape from the QW to the OCL and capture from the OCL to the QW.

The last term in the right-hand side in (A2.1) and (A2.2) is the spontaneous radiative recombination flux in the OCL. The last term in the right-hand side in (A2.5) and (A2.6) is the spontaneous radiative recombination flux in the QW.

In (A2.5) and (A2.9), $w_{\text{n,tunn}}^{L} N_S (1-f_\text{n}) n_{\text{QW}}^{L}$ and $w_{\text{n,tunn}}^{L} n_1^{L,\text{QW}} N_S f_\text{n}$ are the fluxes of electron tunneling from the electron-injecting QW into the QD ensemble and back from the QD ensemble to the QW. The difference $w_{\text{n,tunn}}^{L} N_S (1-f_\text{n}) n_{\text{QW}}^{L} - w_{\text{n,tunn}}^{L} n_1^{L,\text{QW}} N_S f_\text{n}$ is the net in-tunneling flux of electrons from the electron-injecting QW into QDs.

In (A2.6) and (A2.10), $w_{\text{p,tunn}}^{L} p_1^{L,\text{QW}} N_S f_\text{p}$ and $w_{\text{p,tunn}}^{L} N_S (1-f_\text{p}) p_{\text{QW}}^{L}$ are the fluxes of hole tunneling from the QD ensemble to the electron-injecting (i.e., foreign) QW and back from the QW into the QD ensemble. The difference $w_{\text{p,tunn}}^{L} p_1^{L,\text{QW}} N_S f_\text{p} - w_{\text{p,tunn}}^{L} N_S (1-f_\text{p}) p_{\text{QW}}^{L}$ is the net out-tunneling flux of holes from QDs to the electron-injecting QW.

In (A2.9) and (A2.10), $N_S f_\text{n} f_\text{p} / \tau_{\text{QD}}$ is the spontaneous radiative recombination flux in QDs and $\text{v}_\text{g} g^{\max} (f_\text{n} + f_\text{p} - 1) n_{\text{ph}}$ is the stimulated radiative recombination flux.

The first term in the right-hand side in (A2.11) is the rate (in units of s^{-1}) of stimulated emission of photons and the second term is the rate of escape of photons from the cavity through the mirrors.

The flux of electron (and similarly hole) tunneling from a QD ensemble to a QW can be written as

$$w_{\text{n,tunn}} n_1^{\text{QW}} N_S f_\text{n} = N_S \frac{f_\text{n}}{\tau_{\text{n,tunn}}^{\text{QD}\to\text{QW}}}\,, \tag{A2.17}$$

where

$$\tau_{\text{n,tunn}}^{\text{QD}\to\text{QW}} = \frac{1}{w_{\text{n,tunn}} n_1^{\text{QW}}} \tag{A2.18}$$

can be viewed as the tunneling time from a QD to a QW.

The flux of electron tunneling from a QW to a QD ensemble can be written as

$$w_{\text{n,tunn}} N_S (1-f_\text{n}) n_{\text{QW}} = \frac{n_{\text{QW}}}{\tau_{\text{n,tunn}}^{\text{QW}\to\text{QDs}}}\,, \tag{A2.19}$$

where

$$\tau_{\text{n,tunn}}^{\text{QW}\to\text{QDs}} = \frac{\tau_{\text{n,tunn,0}}^{\text{QW}\to\text{QDs}}}{1-f_\text{n}} \tag{A2.20}$$

can be considered as the tunneling time from a QW to a QD ensemble, and

$$\tau_{\mathrm{n,tunn,0}}^{\mathrm{QW\to QDs}} = \frac{1}{w_{\mathrm{n,tunn}} N_S} \tag{A2.21}$$

can be correspondingly considered as the tunneling time into an unoccupied QD ensemble (when $f_{\mathrm{n}} = 0$).

As seen from (A2.18) and (A2.21), the tunneling times $\tau_{\mathrm{n,tunn}}^{\mathrm{QD\to QW}}$ and $\tau_{\mathrm{n,tunn,0}}^{\mathrm{QW\to QDs}}$ are not the same. In contrast to $\tau_{\mathrm{n,tunn}}^{\mathrm{QD\to QW}}$, which describes tunneling from *an individual* QD to a QW, $\tau_{\mathrm{n,tunn,0}}^{\mathrm{QW\to QDs}}$ describes tunneling from a QW to *the entire QD ensemble* — the surface density of QDs, N_S, i.e., a characteristic of the entire QD ensemble, enters into eq. (A2.21) for $\tau_{\mathrm{n,tunn}}^{\mathrm{QW\to QDs}}$. Both $\tau_{\mathrm{n,tunn}}^{\mathrm{QD\to QW}}$ and $\tau_{\mathrm{n,tunn,0}}^{\mathrm{QW\to QDs}}$ are expressed in terms of a single coefficient $w_{\mathrm{n,tunn}}$.

Adding up eqs. (A2.1), (A2.5), and (A2.9), we obtain

$$\frac{\partial}{\partial t}(b_1 n_L + n_{\mathrm{QW}}^L + 2N_S f_{\mathrm{n}}) = \frac{j}{e} - b_1 B n_L p_L - B_{2\mathrm{D}} n_{\mathrm{QW}}^L p_{\mathrm{QW}}^L - N_S \frac{f_{\mathrm{n}} f_{\mathrm{p}}}{\tau_{\mathrm{QD}}} - \mathrm{v}_{\mathrm{g}} g^{\max}(f_{\mathrm{n}} + f_{\mathrm{p}} - 1) n_{\mathrm{ph}}$$
$$- [w_{\mathrm{n,tunn}}^R n_1^{R,\mathrm{QW}} N_S f_{\mathrm{n}} - w_{\mathrm{n,tunn}}^R N_S (1 - f_{\mathrm{n}}) n_{\mathrm{QW}}^R] \tag{A2.22}$$

Adding up eqs. (A2.2) and (A2.6), we obtain

$$\frac{\partial}{\partial t}(b_1 p_L + p_{\mathrm{QW}}^L) = [w_{\mathrm{p,tunn}}^L p_1^{L,\mathrm{QW}} N_S f_{\mathrm{p}} - w_{\mathrm{p,tunn}}^L N_S (1 - f_{\mathrm{p}}) p_{\mathrm{QW}}^L] - b_1 B n_L p_L - B_{2\mathrm{D}} n_{\mathrm{QW}}^L p_{\mathrm{QW}}^L \tag{A2.23}$$

Adding up eqs. (A2.3), (A2.7), and (A2.10), we obtain

$$\frac{\partial}{\partial t}(b_2 p_R + p_{\mathrm{QW}}^R + 2N_S f_{\mathrm{p}}) = \frac{j}{e} - b_2 B n_R p_R - B_{2\mathrm{D}} n_{\mathrm{QW}}^R p_{\mathrm{QW}}^R - N_S \frac{f_{\mathrm{n}} f_{\mathrm{p}}}{\tau_{\mathrm{QD}}} - \mathrm{v}_{\mathrm{g}} g^{\max}(f_{\mathrm{n}} + f_{\mathrm{p}} - 1) n_{\mathrm{ph}}$$
$$- [w_{\mathrm{p,tunn}}^L p_1^{L,\mathrm{QW}} N_S f_{\mathrm{p}} - w_{\mathrm{p,tunn}}^L N_S (1 - f_{\mathrm{p}}) p_{\mathrm{QW}}^L] \tag{A2.24}$$

Adding up eqs. (A2.4) and (A2.8), we obtain

$$\frac{\partial}{\partial t}(b_2 n_R + n_{\mathrm{QW}}^R) = [w_{\mathrm{n,tunn}}^R n_1^{R,\mathrm{QW}} N_S f_{\mathrm{n}} - w_{\mathrm{n,tunn}}^R N_S (1 - f_{\mathrm{n}}) n_{\mathrm{QW}}^R] - b_2 B n_R p_R - B_{2\mathrm{D}} n_{\mathrm{QW}}^R p_{\mathrm{QW}}^R \tag{A2.25}$$

Adding up eqs. (A2.1), (A2.4), (A2.5), (A2.8), and (A2.9), we obtain

$$\frac{\partial}{\partial t}(b_1 n_L + n_{\rm QW}^L + 2N_S f_{\rm n} + b_2 n_R + n_{\rm QW}^R) = \frac{j}{e} - b_1 B n_L p_L - B_{\rm 2D} n_{\rm QW}^L p_{\rm QW}^L - b_2 B n_R p_R - B_{\rm 2D} n_{\rm QW}^R p_{\rm QW}^R - N_S \frac{f_{\rm n} f_{\rm p}}{\tau_{\rm QD}} - {\rm v_g} g^{\max}(f_{\rm n} + f_{\rm p} - 1) n_{\rm ph} \quad \text{(A2.26)}$$

Adding up eqs. (A2.2), (A2.3), (A2.6), (A2.7), and (A2.10), we obtain

$$\frac{\partial}{\partial t}(b_2 p_R + p_{\rm QW}^R + 2N_S f_{\rm p} + b_1 p_L + p_{\rm QW}^L) = \frac{j}{e} - b_1 B n_L p_L - B_{\rm 2D} n_{\rm QW}^L p_{\rm QW}^L - b_2 B n_R p_R - B_{\rm 2D} n_{\rm QW}^R p_{\rm QW}^R - N_S \frac{f_{\rm n} f_{\rm p}}{\tau_{\rm QD}} - {\rm v_g} g^{\max}(f_{\rm n} + f_{\rm p} - 1) n_{\rm ph} \quad \text{(A2.27)}$$

As seen from (A2.26) and (A2.27),

$$\frac{\partial}{\partial t}(b_1 n_L + n_{\rm QW}^L + 2N_S f_{\rm n} + b_2 n_R + n_{\rm QW}^R) = \frac{\partial}{\partial t}(b_2 p_R + p_{\rm QW}^R + 2N_S f_{\rm p} + b_1 p_L + p_{\rm QW}^L), \quad \text{(A2.28)}$$

which gives

$$b_1 n_L + n_{\rm QW}^L + 2N_S f_{\rm n} + b_2 n_R + n_{\rm QW}^R = b_2 p_R + p_{\rm QW}^R + 2N_S f_{\rm p} + b_1 p_L + p_{\rm QW}^L. \quad \text{(A2.29)}$$

Eq. (A2.29) is the condition of global charge neutrality in the structure.

With the assumption of instantaneous tunneling-injection into QDs, we have from (A2.5) and (A2.7),

$$n_{\rm QW}^L = n_1^{L,\rm QW} \frac{f_{\rm n}}{1 - f_{\rm n}} = N_{\rm c}^{\rm 2D} \frac{f_{\rm n}}{1 - f_{\rm n}}, \quad \text{(A2.30)}$$

$$p_{\rm QW}^R = p_1^{R,\rm QW} \frac{f_{\rm p}}{1 - f_{\rm p}} = N_{\rm v}^{\rm 2D} \frac{f_{\rm p}}{1 - f_{\rm p}}. \quad \text{(A2.31)}$$

Eqs. (A2.16) were used in (A2.30) and (A2.31).

With the assumption of instantaneous carrier exchange between the OCL and QW on each side of the structure, we have from (A2.1)-(A2.4),

$$n_L = \frac{n_1}{N_{\rm c}^{\rm 2D}} n_{\rm QW}^L = n_1 \frac{f_{\rm n}}{1 - f_{\rm n}}, \quad \text{(A2.32)}$$

$$p_L = \frac{p_1}{N_{\rm v}^{\rm 2D}} p_{\rm QW}^L, \quad \text{(A2.33)}$$

$$p_R = \frac{p_1}{N_{\mathrm{v}}^{\mathrm{2D}}} p_{\mathrm{QW}}^R = p_1 \frac{f_{\mathrm{p}}}{1-f_{\mathrm{p}}}, \tag{A2.34}$$

$$n_R = \frac{n_1}{N_{\mathrm{c}}^{\mathrm{2D}}} n_{\mathrm{QW}}^R . \tag{A2.35}$$

We used (A2.12) in (A2.32)-(A2.35). We also used eq. (A2.30) in (A2.32) and eq. (A2.31) in (A2.34).

Using (A2.30)-(A2.35) in (A2.22), (A2.23), (A2.25), and (A2.29), we obtain

$$\begin{aligned}\frac{\partial}{\partial t}\left[\left(\frac{b_1 n_1}{N_{\mathrm{c}}^{\mathrm{2D}}}+1\right) N_{\mathrm{c}}^{\mathrm{2D}} \frac{f_{\mathrm{n}}}{1-f_{\mathrm{n}}} + 2N_S f_{\mathrm{n}}\right] &= \frac{j}{e} - \left(\frac{b_1 B n_1 p_1}{N_{\mathrm{c}}^{\mathrm{2D}} N_{\mathrm{v}}^{\mathrm{2D}}} + B_{\mathrm{2D}}\right) N_{\mathrm{c}}^{\mathrm{2D}} \frac{f_{\mathrm{n}}}{1-f_{\mathrm{n}}} p_{\mathrm{QW}}^L \\ &- N_S \frac{f_{\mathrm{n}} f_{\mathrm{p}}}{\tau_{\mathrm{QD}}} - \mathrm{v}_{\mathrm{g}} g^{\max}(f_{\mathrm{n}} + f_{\mathrm{p}} - 1) n_{\mathrm{ph}} - [w_{\mathrm{n,tunn}}^R n_1^{R,\mathrm{QW}} N_S f_{\mathrm{n}} - w_{\mathrm{n,tunn}}^R N_S (1-f_{\mathrm{n}}) n_{\mathrm{QW}}^R]\end{aligned} \tag{A2.36}$$

$$\begin{aligned}\frac{\partial}{\partial t}\left[\left(\frac{b_1 p_1}{N_{\mathrm{v}}^{\mathrm{2D}}}+1\right) p_{\mathrm{QW}}^L\right] &= [w_{\mathrm{p,tunn}}^L p_1^{L,\mathrm{QW}} N_S f_{\mathrm{p}} - w_{\mathrm{p,tunn}}^L N_S (1-f_{\mathrm{p}}) p_{\mathrm{QW}}^L] \\ &- \left(\frac{b_1 B n_1 p_1}{N_{\mathrm{c}}^{\mathrm{2D}} N_{\mathrm{v}}^{\mathrm{2D}}} + B_{\mathrm{2D}}\right) N_{\mathrm{c}}^{\mathrm{2D}} \frac{f_{\mathrm{n}}}{1-f_{\mathrm{n}}} p_{\mathrm{QW}}^L\end{aligned} \tag{A2.37}$$

$$\begin{aligned}\frac{\partial}{\partial t}\left[\left(\frac{b_2 n_1}{N_{\mathrm{c}}^{\mathrm{2D}}}+1\right) n_{\mathrm{QW}}^R\right] &= [w_{\mathrm{n,tunn}}^R n_1^{R,\mathrm{QW}} N_S f_{\mathrm{n}} - w_{\mathrm{n,tunn}}^R N_S (1-f_{\mathrm{n}}) n_{\mathrm{QW}}^R] \\ &- \left(\frac{b_2 B n_1 p_1}{N_{\mathrm{c}}^{\mathrm{2D}} N_{\mathrm{v}}^{\mathrm{2D}}} + B_{\mathrm{2D}}\right) N_{\mathrm{v}}^{\mathrm{2D}} \frac{f_{\mathrm{p}}}{1-f_{\mathrm{p}}} n_{\mathrm{QW}}^R\end{aligned} \tag{A2.38}$$

$$\left(\frac{b_1 n_1}{N_{\mathrm{c}}^{\mathrm{2D}}}+1\right) N_{\mathrm{c}}^{\mathrm{2D}} \frac{f_{\mathrm{n}}}{1-f_{\mathrm{n}}} + 2N_S f_{\mathrm{n}} + \left(\frac{b_2 n_1}{N_{\mathrm{c}}^{\mathrm{2D}}}+1\right) n_{\mathrm{QW}}^R = \left(\frac{b_2 p_1}{N_{\mathrm{v}}^{\mathrm{2D}}}+1\right) N_{\mathrm{v}}^{\mathrm{2D}} \frac{f_{\mathrm{p}}}{1-f_{\mathrm{p}}} + 2N_S f_{\mathrm{p}} + \left(\frac{b_1 p_1}{N_{\mathrm{v}}^{\mathrm{2D}}}+1\right) p_{\mathrm{QW}}^L \tag{A2.39}$$

Using eq. (A2.39), we can express n_{QW}^R in terms of p_{QW}^L, f_{p}, and f_{n} as follows:

$$\begin{aligned} n_{\mathrm{QW}}^R = \frac{1}{\frac{b_2 n_1}{N_{\mathrm{c}}^{\mathrm{2D}}}+1} &\left\{ \left(\frac{b_1 p_1}{N_{\mathrm{v}}^{\mathrm{2D}}}+1\right) p_{\mathrm{QW}}^L \right. \\ &\left. + \left[\left(\frac{b_2 p_1}{N_{\mathrm{v}}^{\mathrm{2D}}}+1\right) N_{\mathrm{v}}^{\mathrm{2D}} \frac{f_{\mathrm{p}}}{1-f_{\mathrm{p}}} + 2N_S f_{\mathrm{p}}\right] - \left[\left(\frac{b_1 n_1}{N_{\mathrm{c}}^{\mathrm{2D}}}+1\right) N_{\mathrm{c}}^{\mathrm{2D}} \frac{f_{\mathrm{n}}}{1-f_{\mathrm{n}}} + 2N_S f_{\mathrm{n}}\right] \right\} \end{aligned} . \tag{A2.40}$$

Eqs. (A2.36), (A2.37), (A2.38), wherein $n_{\rm QW}^{R}$ is given by (A2.40), and eq. (A2.11) present four equations for finding four unknowns – $p_{\rm QW}^{L}$, $f_{\rm p}$, $f_{\rm n}$, and $n_{\rm ph}$.

We can still further simplify our consideration assuming electron-hole symmetry. In such a case, in particular,

$$w_{\rm n,\,tunn}^{R} = w_{\rm p,\,tunn}^{L}, \tag{A2.41}$$

$$n_1^{R,\rm QW} = p_1^{L,\rm QW}, \tag{A2.42}$$

$$f_{\rm n} = f_{\rm p}, \tag{A2.43}$$

$$n_{\rm QW}^{R} = p_{\rm QW}^{L}. \tag{A2.44}$$

Denoting the out-tunneling coefficients $w_{\rm n,\,tunn}^{R} = w_{\rm p,\,tunn}^{L}$ by $w_{\rm out\text{-}tunn}$, the parameters $n_1^{R,\rm QW} = p_1^{L,\rm QW}$ by $F_1^{\rm QW}$, and the minority carrier densities $n_{\rm QW}^{R} = p_{\rm QW}^{L}$ in the foreign QWs by $F_{\rm QW}$, we ultimately arrived at the set of three rate equations (2.1) - (2.3) for finding $f_{\rm n}$, $F_{\rm QW}$, and $n_{\rm ph}$:

Appendix B: Equations (2.1)-(2.3) at the steady state

The dc components $f_{\rm n,0}$, $F_{\rm QW,0}$, and $n_{\rm ph,0}$ are the solutions of rate equations (2.1)-(2.3) at the steady-state ($\partial/\partial t = 0$ in the left-hand side of these equations), which correspond to the dc component j_0 of the injection current density.

Rewriting equations (2.1)- (2.3) at the steady state:

$$0 = \frac{j_0}{e} - \left[\frac{b_1 B n_1^2}{(N_{\rm c}^{\rm 2D})^2} + B_{\rm 2D}\right] N_{\rm c}^{\rm 2D} \frac{f_{\rm n,0}}{1-f_{\rm n,0}} F_{\rm QW,0}$$
$$- N_S \frac{f_{\rm n,0}^2}{\tau_{\rm QD}} - [w_{\rm out-tunn} F_1^{\rm QW} N_S f_{\rm n,0} - w_{\rm out-tunn} N_S (1-f_{\rm n,0}) F_{\rm QW,0}] - {\rm v_g}\, g^{\max}(2f_{\rm n,0}-1) n_{\rm ph,0} \tag{A2.45}$$

$$0 = [w_{\rm out-tunn} F_1^{\rm QW} N_S f_{\rm n,0} - w_{\rm out-tunn} N_S (1-f_{\rm n,0}) F_{\rm QW,0}]$$
$$- \left[\frac{b_1 B n_1^2}{(N_{\rm c}^{\rm 2D})^2} + B_{\rm 2D}\right] N_{\rm c}^{\rm 2D} \frac{f_{\rm n,0}}{1-f_{\rm n,0}} F_{\rm QW,0} \tag{A2.46}$$

$$0 = {\rm v_g}\, g^{\max}(2f_{\rm n,0}-1) n_{\rm ph,0} - {\rm v_g} \beta n_{\rm ph,0} \tag{A2.47}$$

From (A2.47) we have,

$$f_{n,0} = \frac{1}{2}\left(1 + \frac{\beta}{g^{\max}}\right) \tag{A2.48}$$

From (A2.46) we have,

$$F_{QW,0} = \frac{w_{\text{out-tunn}} F_1^{\text{QW}} N_S f_{\text{n},0}}{w_{\text{out-tunn}} N_S \left(1 - f_{n,0}\right) + \left[\frac{b_1 B n_1^2}{(N_{\text{c}}^{\text{2D}})^2} + B_{\text{2D}}\right] N_{\text{c}}^{\text{2D}} \frac{f_{\text{n},0}}{1 - f_{\text{n},0}}} \tag{A2.49}$$

Adding up (A2.45), (A2.46) and (A2.47), we have,

$$0 = \frac{j_0}{e} - 2\left[\frac{b_1 B n_1^2}{(N_{\text{c}}^{\text{2D}})^2} + B_{\text{2D}}\right] N_{\text{c}}^{\text{2D}} \frac{f_{\text{n},0}}{1 - f_{\text{n},0}} F_{\text{QW},0} - N_S \frac{f_{\text{n},0}^2}{\tau_{\text{QD}}} - \text{v}_{\text{g}} \beta n_{\text{ph},0} \tag{A2.50}$$

Introducing the photon lifetime,

$$\tau_{ph} = \frac{1}{\text{v}_{\text{g}} \beta} \tag{A2.51}$$

and the threshold current density,

$$j_{th} = e N_S \frac{f_{\text{n},0}^2}{\tau_{\text{QD}}} + 2e\left[\frac{b_1 B n_1^2}{(N_{\text{c}}^{\text{2D}})^2} + B_{\text{2D}}\right] N_{\text{c}}^{\text{2D}} \frac{f_{\text{n},0}}{1 - f_{\text{n},0}} F_{\text{QW},0} \tag{A2.52}$$

we have from (A2.50)

$$n_{ph,0} = \tau_{ph} \frac{j_0 - j_{th}}{e} \tag{A2.53}$$

Appendix C: Small Signal Analysis

Using (2.4)-(2.7) in (2.1)-(2.3), we will obtain a set of linear algebraic equations in the frequency-dependent small amplitudes $\delta f_{\text{n-m}}$, $\delta F_{\text{QW-m}}$, and $\delta n_{\text{ph-m}}$. The solution of this algebraic set will yield the following equation for the ratio $\delta n_{\text{ph-m}}(\text{i}\omega)/\delta n_{\text{ph-m}}(0)$, defining the response function

$$\frac{\delta n_{ph-m}(i\omega)}{\delta n_{ph-m}(0)} = \frac{C_{13} C_{31} C_{22}(i\omega)}{C_{13} C_{31} C_{22}(i\omega) - i\omega\left[C_{11}(i\omega) C_{22}(i\omega) - C_{12} C_{21}\right]} \;, \tag{A2.54}$$

for which the coefficients C_{ij} are defined as,

$$C_{11}(i\omega)=i\omega\left[\left(\frac{b_1 n_1}{N_c^{2D}}+1\right)N_c^{2D}\frac{1}{\left(1-f_{n,0}\right)^2}+2N_s\right]+\left[\frac{b_1 B n_1^2}{(N_c^{2D})^2}+B_{2D}\right]N_c^{2D}\frac{1}{\left(1-f_{n,0}\right)^2}F_{QW,0}$$
$$+2N_S\frac{f_{n,0}}{\tau_{QD}}+w_{out-tunn}N_S\left(F_1^{QW}+F_{QW,0}\right)+2v_g g^{max}n_{ph,0}$$

(A2.55)

$$C_{12}=\left[\frac{b_1 B n_1^2}{(N_c^{2D})^2}+B_{2D}\right]N_c^{2D}\frac{f_{n,0}}{1-f_{n,0}}-w_{out-tunn}N_S\left(1-f_{n,0}\right)\quad, \tag{A2.56}$$

$$C_{13}=\frac{1}{\tau_{ph}}, \tag{A2.57}$$

$$C_{21}=\left[\frac{b_1 B n_1^2}{(N_c^{2D})^2}+B_{2D}\right]N_c^{2D}\frac{1}{\left(1-f_{n,0}\right)^2}F_{QW,0}-w_{out-tunn}N_S\left(F_1^{QW}+F_{QW,0}\right), \tag{A2.58}$$

$$C_{22}(i\omega)=i\omega\left(\frac{b_1 n_1}{N_c^{2D}}+1\right)+\left[\frac{b_1 B n_1^2}{(N_c^{2D})^2}+B_{2D}\right]N_c^{2D}\frac{f_{n,0}}{1-f_{n,0}}+w_{out-tunn}N_S\left(1-f_{n,0}\right), \tag{A2.59}$$

$$C_{33}=-2v_g g^{max}n_{ph,0}\quad, \tag{A2.60}$$

the coefficients D_{ij} are defined as,

$$D_{11}=\left[\frac{b_1 B n_1^2}{(N_c^{2D})^2}+B_{2D}\right]N_c^{2D}\frac{1}{\left(1-f_{n,0}\right)^2}F_{QW,0}+2N_S\frac{f_{n,0}}{\tau_{QD}}\quad,$$
$$+w_{out-tunn}N_S\left(F_1^{QW}+F_{QW,0}\right)+2v_g g^{max}n_{ph,0}$$

(A2.61)

$$D_{22}=\left[\frac{b_1 B n_1^2}{(N_c^{2D})^2}+B_{2D}\right]N_c^{2D}\frac{f_{n,0}}{1-f_{n,0}}+w_{out-tunn}N_S\left(1-f_{n,0}\right), \tag{A2.62}$$

and for the coefficients Y_i, we have

$$Y_1=\left(\frac{b_1 n_1}{N_c^{2D}}+1\right)N_c^{2D}\frac{1}{\left(1-f_{n,0}\right)^2}+2N_s\quad, \tag{A2.63}$$

$$Y_2=\frac{b_1 n_1}{N_c^{2D}}+1\ , \tag{A2.64}$$

For the cubic equation in ω^2_{-3dB} (eq. 2.11) the coefficients obtained for E are as follows,

$$E_0 = \frac{1}{Y_1^2 Y_2^2}(r-1)C_{13}^2 C_{31}^2 D_{22}^2 \quad , \tag{A2.65}$$

$$E_2 = \frac{1}{Y_1^2 Y_2^2}\left[(C_{12}C_{21} - D_{11}D_{22})^2 - (r-1)Y_2^2 C_{13}^2 C_{31}^2 + 2C_{13}C_{31}(Y_2 C_{12}C_{21} + Y_1 D_{22}^2)\right], \tag{A2.66}$$

$$E_4 = \frac{1}{Y_1^2 Y_2^2}\left[Y_1^2 D_{22}^2 + Y_2^2 D_{11}^2 + 2Y_1 Y_2 (Y_2 C_{13}C_{31} + C_{12}C_{21})\right], \tag{A2.67}$$

REFERENCES

[1] Y. Arakawa and H. Sakaki, “Multidimensional quantum well laser and temperature dependence of its threshold current,” *Appl. Phys. Lett.*, vol. 40, no. 11, pp. 939–941, Jun. 1982.

[2] K. Nishi, R. Mirin, D. Leonard, G. Medeiros-Ribeiro, P. M. Petroff, and A. C. Gossard, “Structural and optical characterization of InAs/InGaAs self-assembled quantum dots grown on (311)*B* GaAs,” *J. Appl. Phys.,* vol. 80, no. 6, pp. 3466–3470, Sept. 1996.

[3] R. Leon, Y. Kim, C. Jagadish, M. Gal, J. Zou, and D. J. H. Cockayne, “Effects of inter-diffusion on the luminescence of InGaAs/GaAs quantum dots,” *Appl. Phys. Lett.*, vol. 69, no. 13, pp. 1888–1890, Sept. 1996.

[4] A. Patanè, A. Polimeni, P. C. Main, M. Henini, and L. Eaves, “High-temperature light emission from InAs quantum dots,” *Appl. Phys. Lett.*, vol. 75, no. 6, pp. 814–816, Aug. 1999.

[5] J. S. Kim and I.-H. Bae, “Optical properties of wetting layer in InAs quantum dots at different growth temperatures,” *J. Korean Phys. Soc.*, vol. 42, no. 92, pp. S483–S486, Feb 2003.

[6] P. Bhattacharya, S. Krishna, J. Phillips, P. J. McCann, and K. Namjou, “Carrier dynamics in self-organized quantum dots and their application to long-wavelength sources and detectors, “ *J. Cryst. Growth,* vols. 227–228, pp. 27-35, July 2001.

[7] N. N. Ledentsov, V. M. Ustinov, A. Yu. Egorov, A. E. Zhukov, M. V. Maksimov, I. G. Tabatadze, and P. S. Kop’ev, “Optical-properties of heterostructures with InGaAs-GaAs quantum clusters,” *Semiconductors*, vol. 28, no. 8, pp. 832–834, Aug. 1994.

[8] N. Kirstädter, N. N. Ledentsov, M. Grundmann, D. Bimberg, V. M. Ustinov, S. S. Ruvimov, M. V. Maximov, P. S. Kop’ev, Zh. I. Alferov, U. Richter, P. Werner, U. Gösele, and J. Heydenreich, “Low threshold, large $T0$ injection laser emission from (InGa)As quantum dots,” *Electron. Lett.*, vol. 30, no. 17, pp. 1416–1417, Aug. 1994.

[9] A. Yu. Egorov, A. E. Zhukov, P. S. Kop’ev, N. N. Ledentsov, M. V. Maksimov, and V. M. Ustinov, “Effect of deposition conditions on the formation of (In,Ga)As quantum clusters in a GaAs matrix,” *Semiconductors*, vol. 28, no. 8, pp. 809–811, Aug. 1994.

[10] Zh. I. Alferov, N. Y. Gordeev, S. V. Zaitsev, P. S. Kop'ev, I. V. Kochnev, V. V. Khomin, I. L. Krestnikov, N. N. Ledentsov, A. V. Lunev, M. V. Maksimov, S. S. Ruvimov, A. V. Sakharov, A. F. Tsatsul'nikov, Y. M. Shernyakov, and D. Bimberg, "A low-threshold injection heterojunction laser based on quantum dots, produced by gas-phase epitaxy from organometallic compounds," *Sov. Phys. Semicond.*, vol. 30, no. 2, pp. 197–200, 1996.

[11] L. V. Asryan and R. A. Suris, "Inhomogeneous line broadening and the threshold current density of a semiconductor quantum dot laser," *Semicond. Sci. Technol.*, vol. 11, no. 4, pp. 554–567, Apr. 1996.

[12] L. V. Asryan and R. A. Suris, "Temperature dependence of the threshold current density of a quantum dot laser," *IEEE J. Quantum Electron.*, vol. 34, pp. 841-850, May 1998.

[13] L. V. Asryan, Y. Wu, and R. A. Suris, "Carrier capture delay and modulation bandwidth in an edge-emitting quantum dot laser," *Appl. Phys. Lett.*, vol. 98, no. 13, Art. no. 131108, Mar. 2011.

[14] V. M. Ustinov, A. Yu. Egorov, A. R. Kovsh, A. E. Zhukov, M. V. Maksimov, A. F. Tsatsul'nikov, N. Y. Gordeev, S. V. Zaitsev, Y. M. Shernyakov, N. A. Bert, P. S. Kop'ev, Zh. I. Alferov, N. N. Ledentsov, J. Böhrer, D. Bimberg, A. O. Kosogov, P. Werner, and U. Gösele, "Low-threshold injection lasers based on vertically coupled quantum dots, " *J. Cryst. Growth,* vol. 175-176, no. 2, pp. 689-685, May. 1997.

[15] N. N. Ledentsov, V. A. Shchukin, M. Grundmann, N. Kirstaedter, J. Bo¨hrer, O. Schmidt, D. Bimberg, V. M. Ustinov, A. Yu. Egorov, A. E. Zhukov, P. S. Kop'ev, S. V. Zaitsev, N. Yu. Gordeev, Zh. I. Alferov, A. I. Borovkov, A. O. Kosogov, S. S. Ruvimov, P. Werner, U. Gosele, and J. Heydenreich, "Direct formation of vertically coupled quantum dots in Stranski-Krastanow growth," *Phys. Rev. B*, vol. 54, no. 12, pp. 8743–8750, Sept. 1996.

[16] A. E. Zhukov, V. M. Ustinov, A. Yu. Egorov, A. R. Kovsh, A. F. Tsatsul'nikov, M. V. Maximov, N. N. Ledentsov, S. V. Zaitsev, N. Y. Gordeev, V. I. Kopchatov, Y. M. Shernyakov, P. S. Kop'ev, D. Bimberg, Zh. I. Alferov, "Injection lasers based on InGaAs quantum dots in an AlGaAs matrix," *J. Electron. Mater.,* vol. 27, no. 3, pp. 106-109, Mar.
1998.

[17] G. Park, O. B. Shchekin, D. L. Huffaker, and D. G. Deppe, "Low threshold oxide-confined 1.3-μm quantum-dot laser," *IEEE Photon. Technol. Lett.*, vol. 33, no. 3, pp. 230–232, Mar.
2000.

[18] D. L. Huffaker, G. Park, Z. Zou, O. B. Shchekin and D. G. Deppe, "1.3 µm room temperature

GaAs-based quantum-dot laser," *Appl. Phys. Lett.*, vol. 73, no. 18, pp. 2564-2566, Nov. 1998.

[19] K. Mukai, Y. Nakata, K. Otsubo, M. Sugawara, N. Yokoyama and H. Ishikawa, "1.3-µm cw lasing of InGaAs-GaAs quantum dots at room temperature with a threshold current of 8 mA," *IEEE Photon. Technol. Lett.*, vol. 11, no. 10, pp. 1205-1207, Oct. 1999.

[20] N. N. Ledentsov, A. R. Kovsh, A. E. Zhukov, N. A. Maleev, S. S. Mikhrin, A. P. Vasil'ev,

E. S. Semenova, M. V. Maximov, Y. M. Shernyakov, N. Kryzhanovskaya, V. Ustinov and D. Bimberg, "High performance quantum dot lasers on GaAs substrates operating in 1.5 µm range," *Electron. Lett.*, vol. 39, no. 15, pp. 1126-1128, Jul. 2003.

[21] H. D. Kim, W. G. Jeong, J. H. Lee, J. S. Yim, D. Lee, R. Stevenson, P. D. Dapkus, J. W. Jang and S. H. Pyun, "Continuous-wave operation of 1.5 µm InGaAs/InGaAsP/InP quantum dot lasers at room temperature," *Appl. Phys. Lett.*, vol. 87, no. 8, Aug. 2005.

[22] K. Kamath, D. Klotzkin, and P. Bhattacharya, “Small-signal modulation characteristics of self-organized quantum dot separate confinement heterostructure and tunneling injection lasers,” *Proc. IEEE LEOS 10th Annual Meeting*, vol. 2, pp. 498–499, Nov. 1997.

[23] P. Bhattacharya, X. K. Zhang, Y. S. Yuan, K. Kamath, D. Klotzkin, C. Caneau, R. Bhat, “High-speed tunnel injection quantum well and quantum dot lasers,” *Proc. SPIE*, vol. 3283, pp. 702–709, Jan. 1998.

[24] P. Bhattacharya and S. Ghosh, “Tunnel injection $In_{0.4}Ga_{0.6}As$/GaAs quantum dot lasers with 15 GHz modulation bandwidth at room temperature,” *Appl. Phys. Lett.*, vol. 80, no. 19, pp. 3482–3484, May 2002.

[25] Y. Qiu, D. Uhl, R. Chacon, and R. Q. Yang, “Lasing characteristics of InAs quantum-dot lasers on (001) InP substrate,” *Appl. Phys. Lett.*, vol. 83, no. 9, pp. 1704–1706, Apr. 2003.

[26] V. Tokranov, M. Yakimov, J. van Eisden, and S. Oktyabrsky, “Tunnel quantum well-on-dots InGaAs-InAs high-gain medium for laser diodes,” *Proc. SPIE*, vol. 6129, pp. 612908-1–612908-10, Jan. 2006.

[27] A. A. George, P. M. Smowton, Z. Mi, and P. Bhattacharya, “Long wavelength quantum-dot lasers selectively populated using tunnel injection,” *Semicond. Sci. Technol.*, vol. 22, pp. 557–560, 2007.

[28] W. Rudno-Rudzinski, G. Sęk, K. Ryczko, M. Syperek, J. Misiewicz, E. S. Semenova, A. Lemaitre, and A. Ramdane, “Room temperature free carrier tunneling in dilute nitride based quantum well - quantum dot tunnel injection system for 1.3 μm,” *Appl. Phys. Lett.*, vol. 94, no. 17, Art. no. 171906, 2009.

[29] E.-M. Pavelescu, C. Gilfert, J. P. Reithmaier, A. Martin-Minguez, and I. Esquivias, “High-power tunnel-injection 1060-nm InGaAs-(Al)GaAs quantum-dot lasers,” IEEE Photon. Technol. Lett., vol. 21, pp. 999–1001, 2009.

[30] L. V. Asryan and S. Luryi, “Tunneling-injection quantum-dot laser: Ultrahigh temperature stability,” *IEEE J. Quantum Electron.*, vol. 37, no. 7, pp. 905–910, Jul. 2001.

[31] L. V. Asryan and S. Luryi, “Temperature-insensitive semiconductor quantum dot laser,” *Solid-State Electron.*, vol. 47, no. 2, pp. 205–212, Feb. 2003.

[32] L. V. Asryan and S. Luryi, “Semiconductor laser with reduced temperature sensitivity,” *U.S. Patent 6 870 178 B2*, Mar. 22, 2005.

[33] T. Chung, G. Walter, and N. Holonyak, “Coupled strained-layer InGaAs quantum-well improvement of an InAs quantum dot AlGaAs-GaAs-InGaAs-InAs heterostructure laser,” *Appl. Phys. Lett.*, vol. 79, no. 27, pp. 4500–4502, Dec. 2001.

[34] G. Walter, T. Chung, and N. Holonyak, “High-gain coupled InGaAs quantum well InAs quantum dot AlGaAs-GaAs-InGaAs heterostructure diode laser operation,” *Appl. Phys. Lett.*, vol. 80, no. 7, pp. 1126–1128, Feb. 2002.

[35] G. Walter, T. Chung, and N. Holonyak, “Coupled-stripe quantum-well-assisted AlGaAs-GaAs-InGaAs-InAs quantum-dot laser,” *Appl. Phys. Lett.*, vol. 80, no. 17, pp. 3045–3047, Apr. 2002.

[36] P. K. Kondratko, S.-L. Chuang, G. Walter, T. Chung, and N. Holonyak, “Observations of near-zero linewidth enhancement factor in a quantum-well coupled quantum-dot laser,” *Appl. Phys. Lett.*, vol. 83, no. 23, pp. 4818–4820, Dec. 2003.

[37] L. V. Asryan, “Modulation bandwidth of a double tunnelling-injection quantum dot laser” *Semiconductor Science and Technology*, Vol. 30(3), 035022, Mar. 2015

[38] L. V. Asryan, S. Luryi and R. A. Suris, “Internal efficiency of semiconductor lasers with a quantum-confined active region,” *IEEE J. Quantum Electron.*, vol. 39, no. 3, pp. 404-418, Mar. 2003.

[39] I. N. Yassievich, K. Schmalz, and M. Beer, “Capture and emission of carriers in semiconductor quantum wells,” *Semicond. Sci. Technol.*, vol. 9, no. 10, pp. 1763–1774, Oct. 1994.

[40] C. Y. Tsai, Y. H. Lo, R. M. Spencer, L. F. Eastman, “Nonlinear gain coefficients in semiconductor quantum-well lasers - effects of carrier diffusion, capture, and escape,” *IEEE J. Select. Topics Quantum Electron.*, vol. 1, no. 2, pp. 316-330, June 1995.

Chapter 3

Effect of Electron-Hole Asymmetry on Modulation Bandwidth of Double Tunneling-Injection Quantum Dot Lasers

Summary

We are focused on modeling the effect of electron-hole asymmetry on modulation bandwidth, we no longer assume that the electron and hole parameters are the same. To purely focus on this effect, we now assume that in every other respect, the DTI QD laser is ideal. We found that there is no reduction in the maximum modulation bandwidth i.e. electron-hole asymmetry does not indicate a reduction in the effectiveness of such a DTI design.

We also note that in cases where electron-hole symmetry must be used (in order to facilitate numerical simplifications), it would be more accurate to use hole parameters instead of electron parameters.

3.1. Introduction

An interesting oversight in most technical discussions on semiconductor lasers and indeed in semiconductors otherwise, is that normally we only use electron parameters in evaluating and modelling device performance and characteristics. It is often implicitly assumed that electron and hole parameters are the same in order to simplify procedures and calculations. It is however well known that they are not. Electron and hole level occupancies obtained self-consistently were shown to be different in [1]. Owing to this inherent asymmetry, there are variations in actual device performance like characteristic temperature [2] and other parameters, from those theoretically calculated using models in which only one set of parameters are used.

The objective here then is twofold.

Firstly, it would be interesting to see the degree of deviation of actual device characteristics owing to electron hole asymmetry. Since our objective here is to ascertain the change in device performance due to this asymmetry alone, the device is assumed to be otherwise ideal.

Secondly, it would be interesting to note which set of parameters (electron or hole) more closely describes the actual device characteristics.

In this regard, studies have previously been conducted for semiconductor quantum-well lasers[3]-[6], however this would be one of the very few of other such studies[7] conducted into quantum-dot lasers.

With these two objectives in mind, the recurrent theme in this chapter will therefore be a comparison in device characteristics of an ideal semiconductor double tunneling-injection quantum-dot laser obtained using: (i) only electron parameters, (ii) only hole parameters and (iii) a model taking into account the inherent electron-hole symmetry.

3.2. Theoretical model

3.2.1. Main assumptions

As we are now focused on modeling the effect of electron-hole asymmetry on modulation bandwidth, we can no longer assume that the electron and hole parameters are the same. To purely focus on this effect, we now assume that in every other respect, the DTI QD laser is ideal, i.e. there is no leakage of carriers by out-tunneling and all carrier exchanges occur instantaneously. Here $w^{R}_{\mathrm{n,\,tunn}}$ and $w^{L}_{\mathrm{p,\,tunn}}$ are zero indicating that tunneling of electrons from a QD to the hole-injecting QW and holes from a QD to the electron-injecting QW does not occur. In this case, we make the following assumptions:

- Carrier exchange between the OCL and injector QWs on each side of the structure is instantaneous ($\mathrm{v}^{L,R}_{\mathrm{n,p,capt}} \to \infty$ and $\tau^{L,R}_{\mathrm{n,p,esc}} \to 0$).
- Tunneling-injection into QDs is instantaneous ($w^{L}_{\mathrm{n,\,tunn}} \to \infty$ and $w^{R}_{\mathrm{p,\,tunn}} \to \infty$).
- Carrier leakage by out-tunneling does not occur (the out-tunneling coefficients $w^{R}_{\mathrm{n,\,tunn}}$ and $w^{L}_{\mathrm{p,\,tunn}}$ are zero)

3.2.2. Modified rate equations model

We have the following set of two rate equations for finding f_{n} and n_{ph}:

$$\frac{\partial}{\partial t}\left(b_1 n_1 \frac{f_{\mathrm{n}}}{1-f_{\mathrm{n}}} + N_c^{2D}\frac{f_{\mathrm{n}}}{1-f_{\mathrm{n}}} + 2N_S f_{\mathrm{n}}\right) = \frac{j}{e} - \\ - N_S \frac{f_n f_p(f_n)}{\tau_{\mathrm{QD}}} - \mathrm{c_g} g^{\max}[f_{\mathrm{n}} + f_p(f_n) - 1]n_{\mathrm{ph}} \quad , \tag{3.1}$$

$$\frac{\partial n_{\mathrm{ph}}}{\partial t} = \mathrm{c_g} g^{\max}[f_{\mathrm{n}} + f_p(f_n) - 1]n_{\mathrm{ph}} - \mathrm{c_g}\beta n_{\mathrm{ph}} \ , \tag{3.2}$$

where,

b_1 thickness of the OCL.

N_S surface density of QDs.

f_n electron level occupancies in QDs

$f_p(f_n)$ hole level occupancies in QDs

τ_{QD} spontaneous radiative lifetime in QD.

c_g group velocity of light,

g^{max} maximum value of the modal gain

n_{ph} 2-D density of photons in the lasing mode (number of photons per unit area of the junction).

N_c^{2D} 2-D effective densities of states in the conduction (and valence band) in the QWs.

n_1 (3-D) effective densities of states in conduction and valence bands in the OCL.

The electron and hole level occupancies are related to each other by the global charge neutrality condition. As such, we can express one as an independent variable (in this case f_n) and the other as the dependent (here $f_p(f_n)$). The charge neutrality condition can as such be given as:

$$b_1 n_1 \frac{f_n}{1-f_n} + N_c^{2D} \frac{f_n}{1-f_n} + 2N_S f_n = b_2 p_1 \frac{f_p}{1-f_p} + N_v^{2D} \frac{f_p}{1-f_p} + 2N_S f_p \ , \tag{3.3}$$

The equations listed have been numerically solved using Mathcad 5. For further analysis of steady state equations, refer to Appendix D.

In Appendix E it is shown that ω_{-3dB_max} is not affected by the electron-hole asymmetry but j_0^{opt} is affected. The effect of the electron-hole asymmetry is incorporated in G^{dif} entering into the expression for j_0^{opt}. Hence, the task is to obtain and compare G^{dif} in the case of the electron-hole asymmetry [eq. (A3.37)] with G^{dif} in the case of the electron-hole symmetry [eq. (A3.38)].

3.3. Effect of electron-hole asymmetry on differential gain (G^{dif}) and non-stimulated differential recombination time

In the general case, we have for G^{dif},

$$G^{dif} = \frac{g^{\max}\left(1 + \frac{df_{p0}}{df_{n0}}\right)}{2Ns + \frac{b_1 n_1 + N_C^{2D}}{\left(1 - f_{n0}\right)^2}} \tag{3.4}$$

In the case of the electron-hole symmetry, G^{dif} from eq. (3.4) will become

$$G^{dif} = \frac{2g^{\max}}{2Ns + \frac{b_1 n_1 + N_C^{2D}}{\left(1 - f_{n0}\right)^2}} \tag{3.5}$$

In the case of the electron-hole asymmetry, it is shown that G^{dif} from eq. (3.4) will become

$$G^{dif} = g^{\max}\left[\frac{1}{2Ns + \frac{b_1 n_1 + N_C^{2D}}{\left(1 - f_{n0}\right)^2}} + \frac{1}{2Ns + \frac{b_2 p_1 + N_V^{2D}}{\left(1 - f_{p0}\right)^2}}\right] \tag{3.6}$$

The given equations have then been numerically evaluated using Mathcad 5. Further analysis of these equations is provided in Appendix E. In Appendix F, it is then proved that L^{min} is not affected by the electron-hole asymmetry. It then becomes possible to derive G^{dif} for the asymptotic cases where L tends to L^{min} and infinity respectively.

Differential gain for the case of L tending to L^{min}

For the case of the electron-hole symmetry, we get the following expression for G^{dif}:

$$G^{dif} \approx \frac{g^{\max}}{2Ns + b_1 n_1 + N_C^{2D}}\left(1 - \frac{L^{\min}}{L}\right) \tag{3.7}$$

For the case of the electron-hole asymmetry, we get

$$G^{dif} \approx \frac{g^{\max}}{\left(b_1 n_1 + N_C^{2D}\right) + \left(b_2 p_1 + N_V^{2D}\right)}\left(1 - \frac{L^{\min}}{L}\right)^2 \tag{3.8}$$

Differential gain for the case of L tending to infinity

For the case of electron-hole symmetry, if L tends to infinity, then

$$f_{n0} = f_{p0} \rightarrow \frac{1}{2} \tag{3.9}$$

we obtain

$$G^{dif} = \frac{g^{\max}}{Ns + 2\left(b_1 n_1 + N_C^{2D}\right)} \tag{3.10}$$

For the case of electron-hole asymmetry, if L tends to infinity (i.e. , β → 0), we have from (A3.40)

$$f_{n0} + f_{p0} = 1 \tag{3.11}$$

or

$$f_{p0} = 1 - f_{n0} \tag{3.12}$$

we finally obtain

$$G^{dif} = \frac{g^{\max}}{Ns + 2\left(b_1 n_1 + N_C^{2D}\right)}\left[1 + \frac{(b_1 n_1 + N_C^{2D}) - (b_2 p_1 + N_V^{2D})}{Ns + 2\left(b_1 n_1 + N_C^{2D}\right)}\right] \tag{3.13}$$

Further analysis of both these cases is provided in Appendix G.

Expressions for non-stimulated differential recombination time

The general expresstion for non-stimulated differential recombination time ($\tau_{non-stim}^{diff}$) can be given by,

$$\tau_{non-stim}^{diff} = \frac{1}{\dfrac{Nsf_{n0}}{\tau_{QD}}\left(\dfrac{f_{p0}}{f_{n0}} + \dfrac{df_{p0}}{df_{n0}}\right)}\left[2Ns + \frac{b_1 n_1 + N_C^{2D}}{\left(1 - f_{n0}\right)^2}\right] \tag{3.14}$$

for the case of electron-hole symmetry, we have from (3.14)

$$\tau_{non-stim}^{diff} = \frac{1}{\frac{f_{n0}}{\tau_{QD}}}\left[1 + \frac{1}{2Ns}\frac{b_1 n_1 + N_C^{2D}}{(1 - f_{n0})^2}\right], \tag{3.15}$$

for the case of electron-hole asymmetry, we have from (3.14)

$$\tau_{non-stim}^{diff} = \frac{1}{\frac{Ns}{\tau_{QD}}} \frac{\left[2Ns + \frac{b_1 n_1 + N_C^{2D}}{(1 - f_{n0})^2}\right]\left[2Ns + \frac{b_1 n_1 + N_V^{2D}}{(1 - f_{p0})^2}\right]}{f_{n0}\left[2Ns + \frac{b_1 n_1 + N_C^{2D}}{(1 - f_{n0})^2}\right] + f_{p0}\left[2Ns + \frac{b_1 n_1 + N_V^{2D}}{(1 - f_{p0})^2}\right]} \tag{3.16}$$

3.4. Discussion

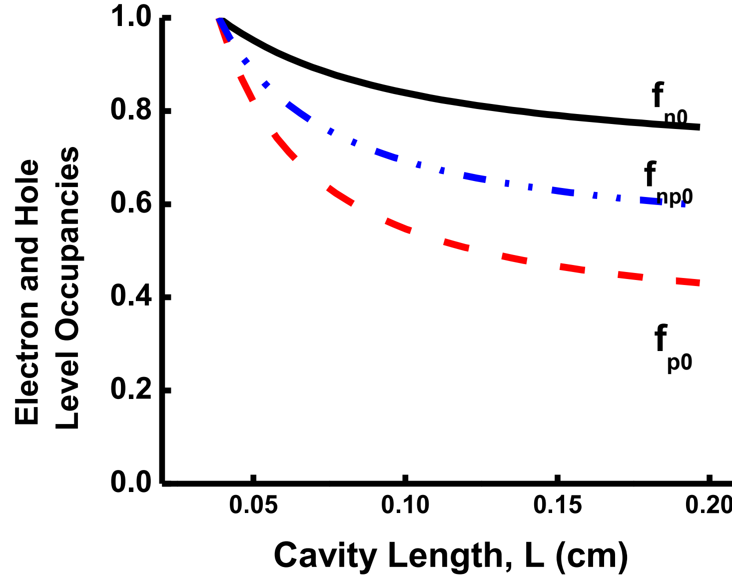

Fig. 3.1. Steady state level occupancies (*f*) vs cavity length (L) for various situations. f_{np0} denotes the level occupancy assuming electron-hole symmetry i.e. both electron and hole occupancies are equal. f_{p0} and f_{n0} represents the level occupancy functions of holes and electrons respectively obtained self-consistently.

In the case of electron-hole symmetry, the electron and hole level occupancy functions are considered to be equal. This is denoted in figure 3.1 as $f_{np,0}$. The justification for this assumption

is that in the limiting case of very small cavity length (close to L equal to L_{min}) both the electron and hole level occupancies converge to unity. However, as cavity length is increased, the level occupancies diverge and they can no longer be assumed to be equal. The electron and hole occupancies are still related.

The electron and hole level occupancies are related to each other by the global charge neutrality condition, as mentioned above in eq. (3.3).

For further analysis of steady state equations and for the quadratic solution to f_p (eq. A3.4), refer to Appendix D.

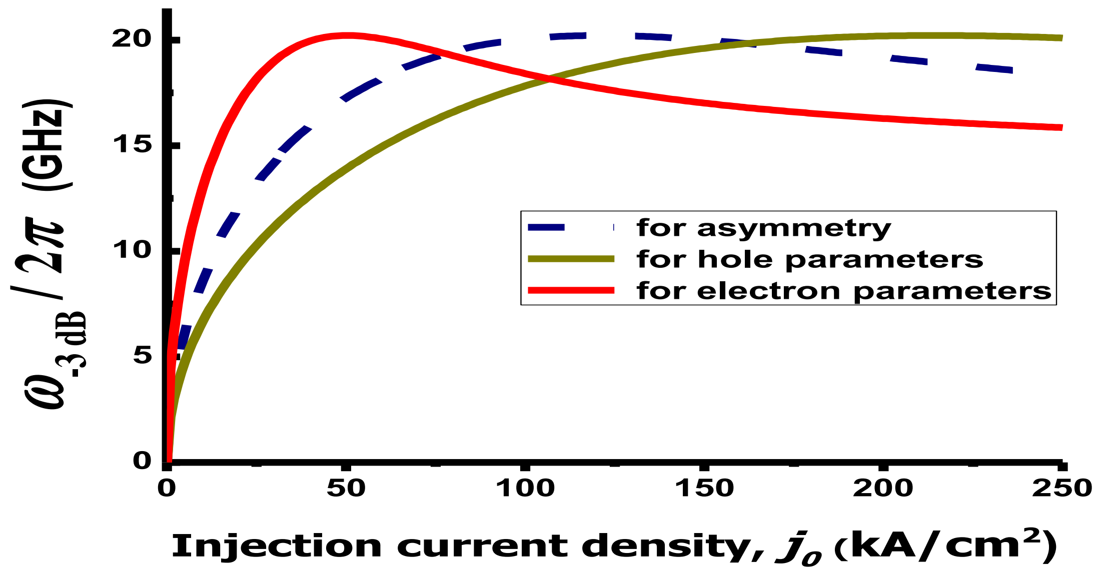

Fig. 3.2. Modulation bandwidth vs dc injection current density (j_0) for three cases electron-hole symmetry using (i) electron parameters, (ii) hole parameters and (iii) for electron-hole asymmetry.

The primary objective of this study is to ascertain whether device parameters calculated considering only using electron parameters and assuming electron-hole symmetry leads to widely inaccurate results. Hence, figure 2.2 illustrating modulation bandwidth vs injection current for the case of electron-hole symmetry and asymmetry is of paramount importance.

The first major takeaway is that for all three curves maximum modulation bandwidth remains the same. This is to be expected, as the maximum modulation bandwidth depends on both,

the effective differential non-stimulated recombination time as well the photon lifetime in the optical cavity. The photon lifetime being much much smaller than the former is the dominating factor, and hence we see no appreciable change in the maximum modulation bandwidth.

However, the optimum injection current varies widely (denoted by the peaks of the curves), the lowest value of j^{opt} being for the case of electron-hole symmetry using electron parameters, the highest for symmetry using hole parameters and the case of asymmetry being in between.

It can be pointed out that from fig. 3.2 we can see that in the case of modulation bandwidth, the actual condition of electron hole asymmetry is closer to the case of symmetry assuming hole parameters than to symmetry using electron parameters.

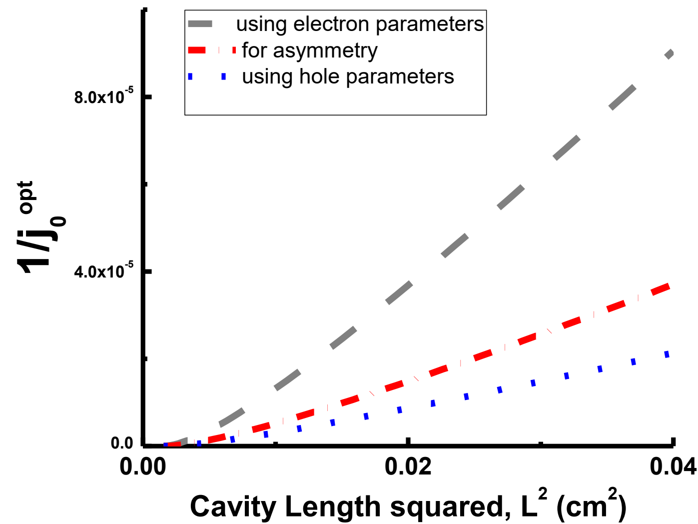

Fig. 3.3. Reciprocal optimum injection current vs cavity length squared (L^2) of QDs for three cases electron-hole symmetry using (i) electron parameters, (ii) hole parameters and (iii) for electron-hole asymmetry.

Fig. 3.3. shows the variation in the optimum injection current for electron-hole symmetry and asymmetry. As fig. 3.3. maps the reciprocal of the optimum current, we see that the curve for electron hole symmetry using electron parameters is the highest, i.e. its actual value is the lowest. The injection current value for electron hole asymmetry is higher and the injection current for the case of electron-hole symmetry using hole parameters is the highest. This reinforces the result obtained in fig. 3.2. where we observed the same phenomena with respect to the optimum injection currents.

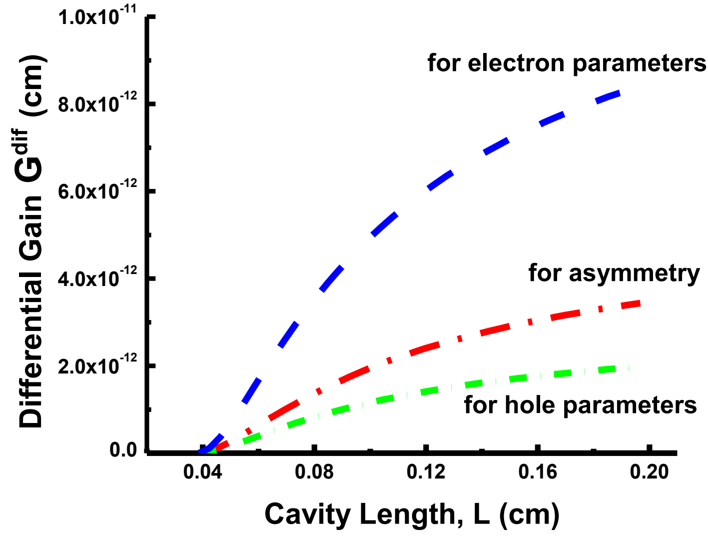

Fig. 3.4. Differential gain (G^{dif}) vs cavity length (L) for three cases electron-hole symmetry using (i) electron parameters, (ii) hole parameters and (iii) for electron-hole asymmetry.

Fig. 3.4. shows the variation in differential gain for electron-hole symmetry and asymmetry. As seen in fig. 3.3. the optimum injection current is affected by the assumption of electron-hole symmetry or asymmetry and this has strong effects on the differential gain. From equation (A3.27) given in Appendix F, we see that the effect of the electron-hole asymmetry is incorporated in the differential gain, entering from the expression for relating the differential gain and the optimum injection current j_0^{opt}.

In fig. 3.4. we see that the differential gain for electron hole symmetry using electron parameters is the highest. The differential gain for electron hole asymmetry is lower and the differential gain for the case of electron-hole symmetry using hole parameters is the lowest. This again reinforces the result obtained in fig. 3.2. where we observed the inverse phenomena with respect to the optimum injection currents which is expected as per equation (A3.27) given in Appendix F.

It is again interesting to note that the actual condition of electron hole asymmetry is closer to the case of symmetry assuming hole parameters than to symmetry using electron parameters.

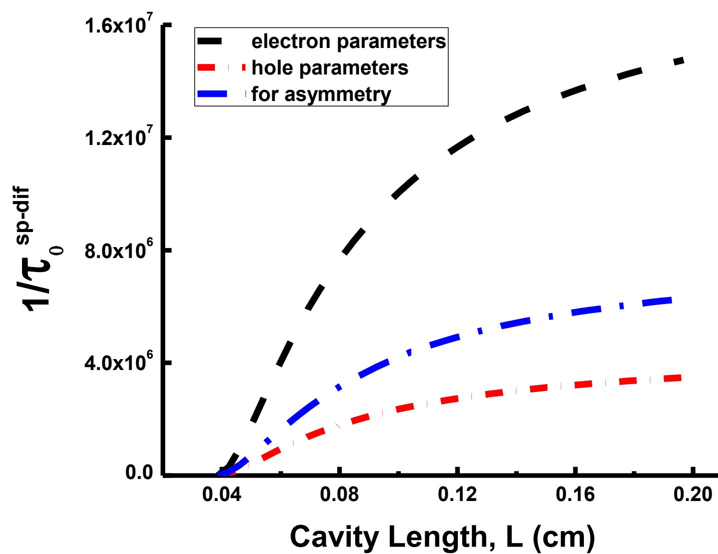

(a)

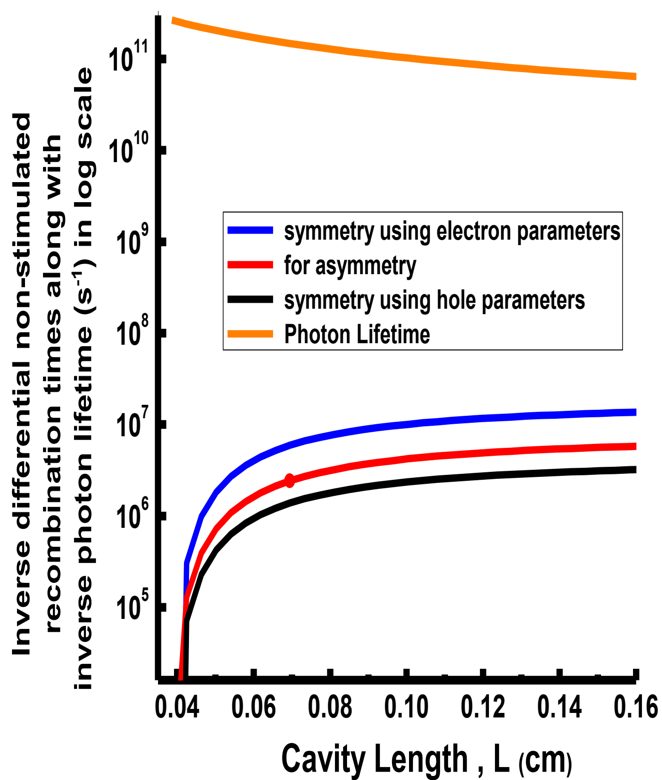

(b)

Fig. 3.5. Fig (a) Reciprocal effective differential non-stimulated recombination time vs cavity length (L) of QDs for three cases electron-hole symmetry using (i)

electron parameters, (ii) hole parameters and (iii) for electron-hole asymmetry. Fig (b) along with the reciprocal photon lifetime in the cavity, plotted in log scale.

The maximum modulation bandwidth depends on both, the effective differential non-stimulated recombination time as well the photon lifetime in the optical cavity. From figure 3.5. (a) we see that the effective differential non-stimulated recombination time does differ, however, from figure (b) we are clearly shown that the photon lifetime, being much much smaller than the former, is the dominating factor It confirms as to why we see no appreciable change in the maximum modulation bandwidth.

3.5. Conclusion

On analyzing the effect of electron-hole asymmetry on the device characteristics of a DTI QD laser, we are confronted with results of significant relevance. It can be noted from the very outset (plots of modulation bandwidth vs injection current) that there is no reduction in the maximum modulation bandwidth i.e. electron-hole asymmetry does not indicate a reduction in the effectiveness of such a DTI design. This is because the maximum modulation bandwidth depends on both, the effective differential non-stimulated recombination time as well the photon lifetime in the optical cavity. The photon lifetime being much much smaller than the former is the dominating factor, and hence we see no appreciable change in the maximum modulation bandwidth.

However, the differential gain varies widely and this has strong effects on the optimum injection current. We see this incorporated in the expression relating differential gain and optimum injection current j_0^{opt} [equation (A3.27) given in Appendix F].

We also see that the actual condition i.e. that of electron hole asymmetry is among the cases of symmetry better represented assuming hole parameters than using electron parameters. As such, in cases where electron-hole symmetry must be used (in order to facilitate numerical simplifications), it would be more accurate to use hole parameters instead of electron parameters.

Appendix D: Steady State Solutions

At steady state, from eq. (3.1) and (3.2), we have:

$$0 = \frac{j}{e} - N_S \frac{f_{n0} f_{p0}(f_{n0})}{\tau_{\mathrm{QD}}} - \mathrm{c_g} g^{\max} [f_{\mathrm{n0}} + f_{p0}(f_{n0}) - 1] n_{\mathrm{ph}} \quad , \tag{A3.1}$$

$$0 = \mathrm{c_g} g^{\max} [f_{\mathrm{n0}} + f_{p0}(f_{n0}) - 1] n_{\mathrm{ph}} - \mathrm{c_g} \beta n_{\mathrm{ph}} \quad , \tag{A3.2}$$

From (3.2), we get the following condition to find f_{n0} :

$$f_{\mathrm{n0}} + f_{p0}(f_{n0}) - 1 = \frac{\beta}{g^{\max}} \quad , \tag{A3.3}$$

Solving the equations (A3.1) and (A3.3), $f_{p0}(f_{n0})$ is given by (A3.4) [or equivalently, (A3.5)]

$$f_p = \frac{1}{2} \left\{ \begin{array}{l} (1 + f_n) + \dfrac{b_2 p_1 + N_V^{2D}}{2Ns} + \dfrac{b_1 n_1 + N_C^{2D}}{2Ns} \dfrac{f_n}{1 - f_n} - \\ \sqrt{\left[(1 + f_n) + \dfrac{b_2 p_1 + N_V^{2D}}{2Ns} + \dfrac{b_1 n_1 + N_C^{2D}}{2Ns} \dfrac{f_n}{1 - f_n} \right]^2 - 4 \left(\dfrac{b_1 n_1 + N_C^{2D}}{2Ns} \dfrac{f_n}{1 - f_n} + f_n \right)} \end{array} \right\} \tag{A3.4}$$

We can write (A3.4) as follows:

$$f_p = \frac{2 \left(\dfrac{b_1 n_1 + N_C^{2D}}{2Ns} \dfrac{f_n}{1 - f_n} + f_n \right)}{\left\{ \begin{array}{l} (1 + f_n) + \dfrac{b_2 p_1 + N_V^{2D}}{2Ns} + \dfrac{b_1 n_1 + N_C^{2D}}{2Ns} \dfrac{f_n}{1 - f_n} + \\ \sqrt{\left[(1 + f_n) + \dfrac{b_2 p_1 + N_V^{2D}}{2Ns} + \dfrac{b_1 n_1 + N_C^{2D}}{2Ns} \dfrac{f_n}{1 - f_n} \right]^2 - 4 \left(\dfrac{b_1 n_1 + N_C^{2D}}{2Ns} \dfrac{f_n}{1 - f_n} + f_n \right)} \end{array} \right\}} \tag{A3.5}$$

For the number of photons obtained, we have

$$n_{\mathrm{ph}} = \tau_{ph} \left[\frac{j_0}{e} - N_S \frac{f_{n0} f_{p0}(f_{n0})}{\tau_{\mathrm{QD}}} \right] \quad , \tag{A3.6}$$

where,

$$\tau_{ph} = \frac{1}{c_g \beta} \quad , \tag{A3.7}$$

or, introducing the threshold current density,

$$j_{th} = eN_S \frac{f_{n0} f_{p0}(f_{n0})}{\tau_{\mathrm{QD}}} \quad , \tag{A3.8}$$

we have

$$n_{\mathrm{ph},0} = \tau_{\mathrm{ph}} \frac{j_0 - j_{th}}{\tau_{\mathrm{QD}}} \quad , \tag{A3.9}$$

We can write eqs. (3.1), (3.2) as follows:

$$\frac{\partial n}{\partial t} = \frac{j}{e} - F_{non-stim} - F_{stim} \quad , \tag{A3.10}$$

$$\frac{\partial n_{ph}}{\partial t} = F_{stim} - F_{loss} \quad , \tag{A3.11}$$

where we introduced the total electron density per unit area of the junction,

$$n = b_1 n_1 \frac{f_{\mathrm{n}}}{1 - f_{\mathrm{n}}} + N_c^{2D} \frac{f_{\mathrm{n}}}{1 - f_{\mathrm{n}}} + 2N_S f_{\mathrm{n}} \quad , \tag{A3.12}$$

and the fluxes [in units of $\mathrm{cm}^{-2}.\mathrm{s}^{-1}$] of the corresponding processes,

$$F_{non-stim} = N_S \frac{f_n f_p(f_n)}{\tau_{\mathrm{QD}}} \quad , \tag{A3.13}$$

$$F_{stim} = c_g g^{\max}[f_{\mathrm{n}} + f_p(f_n) - 1] n_{\mathrm{ph}} \quad , \tag{A3.14}$$

$$F_{loss} = c_g \beta n_{\mathrm{ph}} , \tag{A3.15}$$

Appendix E: Modulation Response

Applying the small-signal analysis to eqs. (A3.10) and (A3.11), we will find:

$$H(\omega) = \frac{\omega_0^4}{(\omega^2 - \omega_0^2) + 4\Gamma_{dec}^2 \omega^2} , \tag{A3.16}$$

where

$$\omega_0 = \sqrt{c_g \beta n_{ph} \frac{1}{\tau_{ph}}}\,, \tag{A3.17}$$

$$\Gamma_{dec} = \frac{1}{2}\left(\frac{1}{\tau_{non-stim}^{dif}} + c_g \beta n_{ph}\right), \tag{A3.18}$$

$$G^{dif} = \frac{dg_0}{dn_0} = \frac{dg_0}{df_{n0}} \frac{1}{\frac{dn_0}{df_{n0}}}\,, \tag{A3.19}$$

$$\frac{1}{\tau_{non-stim}^{dif}} = \frac{dF_{non-stim,0}}{dn_0} = \frac{dF_{non-stim,0}}{df_{n0}} \frac{1}{\frac{dn_0}{df_{n0}}}\,, \tag{A3.20}$$

$$g_0 = g^{\max}\left[f_{n0} + f_{p0}(f_{n0}) - 1\right], \tag{A3.21}$$

The modulation bandwidth $\boldsymbol{w}_{-3dB}$ is found from the following equation:

$$10 \log_{10} H(\omega_{-3dB}) = -3, \tag{A3.22}$$

Using (A3.16) in (A3.22) we have obtained the following expression for ω_{-3dB} :

$$\omega_{-3dB} = \sqrt{\left(\omega_0^2 - 2\Gamma_{dec}^2\right) + \sqrt{\left(\omega_0^2 - 2\Gamma_{dec}^2\right)^2 + (r-1)\omega_0^4}}\,, \tag{A3.23}$$

where

$$r = 10^{0.3} \approx 1.995 \tag{A3.24}$$

As a function of $\boldsymbol{j}_0$, $\boldsymbol{w}_{-3dB}$ has a maximum. The maximum is obtained at :

$$j_0^{opt} = j_{th} + \frac{2e}{c_g G^{dif} \tau_{ph}^2}\left(\frac{1}{2} - \frac{1}{2}\frac{\tau_{ph}}{\tau_{non-stim}^{dif}} + \frac{1}{2}\sqrt{1 - 2\frac{\tau_{ph}}{\tau_{non-stim}^{dif}}}\right), \tag{A3.25}$$

and is equal to

$$\omega_{-3dB}^{\max} = \sqrt[4]{r-1}\,\frac{\sqrt{2}}{\tau_{ph}}\sqrt{\frac{1}{2} - \frac{1}{2}\frac{\tau_{ph}}{\tau_{non-stim}^{dif}} + \frac{1}{2}\sqrt{1 - 2\frac{\tau_{ph}}{\tau_{non-stim}^{dif}}}}\,, \tag{A3.26}$$

In the case of electron-hole symmetry and asymmetry for $L \geq L^{min}$

$$\tau_{ph} \leq\leq \tau_{non-stim}^{dif}$$

and the equations (A3.25) and (A3.26) become

$$j_0^{opt} = \frac{2e}{c_g G^{dif} \tau_{ph}^2}, \tag{A3.27}$$

$$\omega_{-3dB}^{\max} = \sqrt[4]{r-1}\,\frac{\sqrt{2}}{\tau_{ph}}, \tag{A3.28}$$

Effect of electron-hole asymmetry on G^{dif}

For the total derivative, which enters into (A3.19), we have

$$\frac{dg_0}{df_{n0}} = \frac{\partial g_0}{\partial f_{n0}} + \frac{\partial g_0}{\partial f_{p0}}\frac{\partial f_{p0}}{\partial f_{n0}} = g^{\max}\left(1 + \frac{df_{p0}}{df_{n0}}\right), \tag{A3.29}$$

In the case of electron-hole symmetry,

$$\frac{df_{p0}}{df_{n0}} = 1 , \tag{A3.30}$$

and

$$1 + \frac{df_{p0}}{df_{n0}} = 2 , \tag{A3.31}$$

For the total derivative which enters into (21), we have

$$\frac{dF_{non-stim,0}}{df_{n0}} = \frac{\partial F_{non-stim,0}}{\partial f_{n0}} + \frac{\partial F_{non-stim,0}}{\partial f_{p0}}\frac{\partial f_{p0}}{\partial f_{n0}} = \frac{Nsf_{p0}}{\tau_{QD}} + \frac{Nsf_{n0}}{\tau_{QD}}\frac{df_{p0}}{df_{n0}} = \frac{Nsf_{n0}}{\tau_{QD}}\left(\frac{f_{p0}}{f_{n0}} + \frac{df_{p0}}{df_{n0}}\right), \tag{A3.32}$$

In the case of the electron-hole symmetry, the expressions in the brackets in the right hand side of (A3.29) and (A3.32) become equal to 2 [from eq. (A3.31)] and as

$$\frac{f_{p0}}{f_{n0}} + \frac{df_{p0}}{df_{n0}} = 2 , \tag{A3.33}$$

Finding the expression of $\frac{df_{p0}}{df_{n0}}$ from (3.3), by rewriting (3.3) as

$$\left(b_1 n_1 + N_c^{2D}\right)\frac{f_n}{1-f_n} + 2N_S f_n = \left(b_2 p_1 + N_V^{2D}\right)\frac{f_p}{1-f_p} + 2N_S f_p, \tag{A3.34}$$

we have from (A3.34),

$$\left[\left(b_1 n_1 + N_c^{2D}\right)\frac{1}{\left(1-f_{\mathrm{n}}\right)^2} + 2N_S\right]df_{\mathrm{n}} = \left[\left(b_2 p_1 + N_V^{2D}\right)\frac{1}{\left(1-f_{\mathrm{p}}\right)^2} + 2N_S\right]df_{\mathrm{p}}$$

Hence, we have

$$\frac{df_{\mathrm{n}}}{df_{\mathrm{p}}} = \frac{\dfrac{\left(b_1 n_1 + N_c^{2D}\right)}{\left(1-f_{\mathrm{n}}\right)^2} + 2N_S}{\dfrac{\left(b_2 p_1 + N_V^{2D}\right)}{\left(1-f_{\mathrm{p}}\right)^2} + 2N_S}\ , \tag{A3.35}$$

Equation (A3.35) holds true for both time dependent and steady state $\boldsymbol{f}_{\mathrm{p}}$ and $\boldsymbol{f}_{\mathrm{n}}$. The expression for $\boldsymbol{f}_{\mathrm{p}}$ in terms of $\boldsymbol{f}_{\mathrm{n}}$ is given by (A3.4) [or equivalently by (A3.5)].

As seen from (A3.27), the effect of the electron-hole asymmetry on $\boldsymbol{j}^{\mathrm{opt}}{}_0$ is related to that on G^{dif}. We calculated G^{dif} using (A3.19). From (A3.12), we have

$$\frac{dn_0}{df_{n0}} = 2Ns + \frac{b_1 n_1 + N_C^{2D}}{\left(1-f_{n0}\right)^2}\ , \tag{A3.36}$$

Using (A3.29) and (A3.36) in (A3.19), we have for G^{dif},

$$G^{dif} = \frac{g^{\max}\left(1+\dfrac{df_{p0}}{df_{n0}}\right)}{2Ns + \dfrac{b_1 n_1 + N_C^{2D}}{\left(1-f_{n0}\right)^2}} \tag{A3.37}$$

In the case of the electron-hole symmetry, (A3.37) will become

$$G^{dif} = \frac{2g^{\max}}{2Ns + \dfrac{b_1 n_1 + N_C^{2D}}{\left(1-f_{n0}\right)^2}} \tag{A3.38}$$

where

$$f_{\mathrm{n}0} = f_{p0} = \frac{1}{2}\left(1+\frac{\beta}{g^{\max}}\right) = \frac{1}{2}\left(1+\frac{L^{\min}}{L}\right) \tag{A3.39}$$

In the case of electron-hole asymmetry, $f_{\mathrm{n}0}$ should be found from the steady state lasing condition

$$g^{\max}\left[f_{n0}+f_{p0}(f_{n0})-1\right]=\beta \tag{A3.40}$$

With (A3.35), eq. (A3.37) for G^{dif} in the case of electron-hole asymmetry can be written as

$$G^{dif}=g^{\max}\left[\frac{1}{2Ns+\dfrac{b_1 n_1+N_C^{2D}}{\left(1-f_{n0}\right)^2}}+\frac{1}{2Ns+\dfrac{b_2 p_1+N_V^{2D}}{\left(1-f_{p0}\right)^2}}\right] \tag{A3.41}$$

Appendix F: Proof that L^{min} is unaffected by the electron-hole asymmetry

Let us check whether L^{min} is affected by the electron-hole asymmetry,

$$\beta^{\max}=g^{\max} \tag{A3.42}$$

and hence

$$L^{\min}=\frac{1}{g^{\max}}\ln\frac{1}{R} \tag{A3.43}$$

Let us assume that, in the case of the electron-hole asymmetry too, β^{max} and L^{min} are given by (A3.42) and (A3.43). From (A3.40), we have

$$f_{n0}+f_{p0}(f_{n0})=2 \tag{A3.44}$$

which necessarily means that

$$f_{n0}=f_{p0}=1 \tag{A3.45}$$

as in the case of electron-hole symmetry.

Let us show, using (A3.5), that indeed f_{p0} tends to unity if f_{n0} tends to unity. If f_{n0} tends to unity we have from (A3.5) [keeping just the largest terms both in the numerator and the denominator],

$$f_p=\frac{2\dfrac{b_1 n_1+N_C^{2D}}{2Ns}\dfrac{f_n}{1-f_n}}{\dfrac{b_1 n_1+N_C^{2D}}{2Ns}\dfrac{f_n}{1-f_n}+\dfrac{b_1 n_1+N_C^{2D}}{2Ns}\dfrac{f_n}{1-f_n}}=1 \tag{A3.46}$$

Hence, we proved that L^{min} is not affected by the electron-hole asymmetry and is given by (A3.43). When L tends to L^{min}, both f_n and f_p go to 1.

Let us find the asymptotic expressions for f_{n0} and f_{p0} when L tends to L^{min}. In this case both f_{n0} and f_{p0} tend to converge to unity with just small deviations. Let us write f_{n0} and f_{p0} in the form

$$f_{n0} = 1 - y_1 \tag{A3.47}$$

$$f_{p0} = 1 - y_2 \tag{A3.48}$$

where y_1 and y_2 are small quantities.

Using (A3.47) and (A3.48) in (A3.40), we have

$$g^{max}(1 - y_1 - y_2) = \frac{1}{L}\ln\frac{1}{R}$$

or

$$g^{max} - g^{max}(y_1 + y_2) = \frac{1}{L^{min}}\ln\frac{1}{R} + \left(\frac{1}{L} - \frac{1}{L^{min}}\right)\ln\frac{1}{R} \tag{A3.49}$$

Taking into account that

$$g^{max} = \frac{1}{L^{min}}\ln\frac{1}{R} \quad ,$$

$$\frac{1}{L^{min}}(y_1 + y_2) = \frac{1}{L^{min}} - \frac{1}{L}$$

or

$$y_1 + y_2 = 1 - \frac{L^{min}}{L} \tag{A3.50}$$

Let us now use (A3.47) and (A3.48) in (A3.34). We have [keeping the largest terms in both sides of (A3.34)]

$$\frac{b_1 n_1 + N_C^{2D}}{y_1} = \frac{b_2 p_1 + N_V^{2D}}{y_2} \tag{A3.51}$$

Hence, we have from (A3.51),

$$y_2 = \frac{b_2 p_1 + N_V^{2D}}{b_1 n_1 + N_C^{2D}}\, y_1 \tag{A3.52}$$

Putting (A3.52) in (A3.50), we have

$$\left(1+\frac{b_2 p_1 + N_V^{2D}}{b_1 n_1 + N_C^{2D}}\right) y_1 = 1 - \frac{L^{\min}}{L}$$

Hence, we have

$$y_1 = \frac{b_1 n_1 + N_C^{2D}}{\left(b_1 n_1 + N_C^{2D}\right) + \left(b_2 p_1 + N_V^{2D}\right)} \left(1 - \frac{L^{\min}}{L}\right) \quad \text{(A3.53)}$$

$$y_2 = \frac{b_2 p_1 + N_V^{2D}}{\left(b_1 n_1 + N_C^{2D}\right) + \left(b_2 p_1 + N_V^{2D}\right)} \left(1 - \frac{L^{\min}}{L}\right) \quad \text{(A3.54)}$$

Hence, we finally have for L tending to L^{min}

$$f_{n0} = 1 - \frac{b_1 n_1 + N_C^{2D}}{\left(b_1 n_1 + N_C^{2D}\right) + \left(b_2 p_1 + N_V^{2D}\right)} \left(1 - \frac{L^{\min}}{L}\right) \quad \text{(A3.55)}$$

$$f_{p0} = 1 - \frac{b_2 p_1 + N_V^{2D}}{\left(b_1 n_1 + N_C^{2D}\right) + \left(b_2 p_1 + N_V^{2D}\right)} \left(1 - \frac{L^{\min}}{L}\right) \quad \text{(A3.56)}$$

As seen from (A3.27) and (A3.28), w_{-3dB_max} is not affected by the electron-hole asymmetry but j_0^{opt} is affected. The effect of the electron-hole asymmetry is incorporated in G^{dif} entering into the expression for j_0^{opt}. Hence, the task is to compare G^{dif} in the case of the electron-hole asymmetry [eq. (A3.37)] with G^{dif} in the case of the electron-hole symmetry [eq. (A3.38)].

Appendix G: Differential gain for the case of L tending to L^{min}

For the case of the electron-hole symmetry, using (A3.39) in (A3.38) gives the following expression for G^{dif}:

$$G^{dif} \approx \frac{g^{\max}}{2Ns + b_1 n_1 + N_C^{2D}} \left(1 - \frac{L^{\min}}{L}\right) \quad \text{(A3.57)}$$

For the case of the electron-hole asymmetry, using (A3.55) and (A3.56) in (A3.41) gives

$$G^{dif} \approx \frac{g^{\max}}{\left(b_1 n_1 + N_C^{2D}\right) + \left(b_2 p_1 + N_V^{2D}\right)} \left(1 - \frac{L^{\min}}{L}\right)^2 \quad \text{(A3.58)}$$

Equation (A3.58) can also be obtained from (A3.37). Let us show this in the following manner

$$\frac{df_{p0}}{df_{n0}} = \frac{df_{p0}}{dL}\frac{dL}{df_{n0}} = \frac{\dfrac{df_{p0}}{dL}}{\dfrac{df_{n0}}{dL}} \qquad \text{(A3.59)}$$

Using (A3.55) and (A3.56) in (A3.59) gives

$$\frac{df_{p0}}{df_{n0}} \approx \frac{b_2 p_1 + N_V^{2D}}{b_1 n_1 + N_C^{2D}} \qquad \text{(A3.60)}$$

Now using (A3.55) and (A3.60) in (A3.37) gives us (A3.58).

Differential gain for the case of L tending to infinity

For the case of electron-hole symmetry, if L tends to infinity, then

$$f_{n0} = f_{p0} \to \frac{1}{2} \qquad \text{(A3.61)}$$

Using (A3.61) in (A3.38) gives

$$G^{dif} = \frac{g^{\max}}{Ns + 2\left(b_1 n_1 + N_C^{2D}\right)} \qquad \text{(A3.62)}$$

For the case of electron-hole asymmetry, if L tends to infinity (i.e. , $\beta \to 0$), we have from (A3.40)

$$f_{n0} + f_{p0} = 1 \qquad \text{(A3.63)}$$

or

$$f_{p0} = 1 - f_{n0} \qquad \text{(A3.64)}$$

Using (A3.64) in (3.3), we will obtain a cubic equation for finding f_{n0}; the same equation will be obtained if we use (A3.64) in (A3.5).

Let us assume that the electron-hole asymmetry is slight, i.e. the difference

$$\delta = \left(b_2 p_1 + N_V^{2D}\right) - \left(b_1 n_1 + N_C^{2D}\right) \qquad \text{(A3.65)}$$

is small. Denoting

$$A = b_1 n_1 + N_C^{2D} \tag{A3.66}$$

we have,

$$b_2 p_1 + N_V^{2D} = A + \delta \tag{A3.67}$$

It is clear that, in this case of slight electron-hole asymmetry and L tending to infinity, the deviations of f_{n0} and f_{p0} from ½ (the case of electron-hole symmetry) should be small. To satisfy (A3.63), f_{n0} and f_{p0} should be written as

$$f_{n0} = \frac{1}{2} + \Delta \tag{A3.68}$$

$$f_{p0} = \frac{1}{2} - \Delta \tag{A3.69}$$

where Δ is a small quantity of the order of δ (i.e. linear in δ). The expression for Δ in terms of δ can be obtained using (A3.67)-(A3.69) in (3.3). Prior to doing this let us simplify the expression (A3.41) for G^{dif} using (A3.67)-(A3.69). The expression in the square brackets in (A3.41) is

$$\frac{1}{2Ns + \dfrac{A}{\left(\dfrac{1}{2} - \Delta\right)^2}} + \frac{1}{2Ns + \dfrac{A+\delta}{\left(\dfrac{1}{2} + \Delta\right)^2}} \approx \frac{1}{2Ns + \dfrac{A}{\dfrac{1}{4} - \Delta}} + \frac{1}{2Ns + \dfrac{A+\delta}{\dfrac{1}{4} + \Delta}} =$$

$$= \frac{1}{2Ns + \dfrac{4A}{1-4\Delta}} + \frac{1}{2Ns + \dfrac{4(A+\delta)}{1+4\Delta}} \approx \frac{1}{2Ns + 4A(1+4\Delta)} + \frac{1}{2Ns + 4(A+\delta)(1-4\Delta)} \approx$$

$$\approx \frac{1}{(2Ns+4A)+16A\Delta} + \frac{1}{(2Ns+4A)-16A\Delta+4\delta} =$$

$$= \frac{1}{2Ns+4A}\left[\frac{1}{1+\dfrac{8A\Delta}{Ns+2A}} + \frac{1}{1-\dfrac{8A\Delta-2\delta}{Ns+2A}}\right] \approx \frac{1}{2Ns+4A}\left[1-\frac{8A\Delta}{Ns+2A}+1+\frac{8A\Delta-2\delta}{Ns+2A}\right] =$$

$$= \frac{1}{Ns+2A}\left(1-\frac{\delta}{Ns+2A}\right)$$

(A3.70)

As we see, Δ does not enter into (A3.70) and hence, to find G^{dif}, we do not need to find Δ in terms of δ from eq. (3.3)

Hence we have,

$$G^{dif} = \frac{g^{\max}}{Ns + 2A}\left(1 - \frac{\delta}{Ns + 2A}\right) \tag{A3.71}$$

and finally,

$$G^{dif} = \frac{g^{\max}}{Ns + 2\left(b_1 n_1 + N_C^{2D}\right)}\left[1 + \frac{(b_1 n_1 + N_C^{2D}) - (b_2 p_1 + N_V^{2D})}{Ns + 2\left(b_1 n_1 + N_C^{2D}\right)}\right] \tag{A3.72}$$

Appendix H: Expressions for non-stimulated differential recombination time

Using (A3.20), (A3.32) and (A3.36) we have ,

$$\tau_{non-stim}^{diff} = \frac{1}{\dfrac{Nsf_{n0}}{\tau_{QD}}\left(\dfrac{f_{p0}}{f_{n0}} + \dfrac{df_{p0}}{df_{n0}}\right)}\left[2Ns + \frac{b_1 n_1 + N_C^{2D}}{\left(1 - f_{n0}\right)^2}\right] \tag{A3.73}$$

Using (A3.33) from the case of electron-hole symmetry, we have from (A3.73)

$$\tau_{non-stim}^{diff} = \frac{1}{\dfrac{f_{n0}}{\tau_{QD}}}\left[1 + \frac{1}{2Ns}\frac{b_1 n_1 + N_C^{2D}}{\left(1 - f_{n0}\right)^2}\right], \tag{A3.74}$$

Using (A3.35) for the case of electron-hole asymmetry, we have from (A3.73)

$$\tau_{non-stim}^{diff} = \frac{1}{\dfrac{Ns}{\tau_{QD}}}\frac{\left[2Ns + \dfrac{b_1 n_1 + N_C^{2D}}{\left(1 - f_{n0}\right)^2}\right]\left[2Ns + \dfrac{b_1 n_1 + N_V^{2D}}{\left(1 - f_{p0}\right)^2}\right]}{f_{n0}\left[2Ns + \dfrac{b_1 n_1 + N_C^{2D}}{\left(1 - f_{n0}\right)^2}\right] + f_{p0}\left[2Ns + \dfrac{b_1 n_1 + N_V^{2D}}{\left(1 - f_{p0}\right)^2}\right]} \tag{A3.75}$$

References

[1] L. V. Asryan and R. A. Suris, "Charge Neutrality Violation in Quantum-Dot Laser", IEEE Journal of Selected Topics in Quantum Electronics, Vol. 3, Number 2, April 1997

[2]L. V. Asryan and R. A. Suris, "Characteristic temperature of quantum dot laser", Electronics Letters, 23rd October 1997 Vol. 33 No. 22

[3] L. V. Asryan and Z. N. Sokolova, "Optical power of semiconductor lasers with a low-dimensional active region", *Journal of Applied Physics*, Vol. 115, issue 2, 023107, Jan 2014

[4] Z. N. Sokolova, I. S. Tarasov and L. V. Asryan, "Threshold characteristics of semiconductor lasers under conditions of violation of electroneutrality in quantum wells", *Quantum Electronics*, Vol. 43(5), pp 428–432, 2013.

[5] Z. N. Sokolova, N. A. Pikhtin, I. S. Tarasov and L. V. Asryan, "Threshold characteristics of a semiconductor quantum-well laser: inclusion of global electroneutrality in the structure", *Quantum Electronics*, Vol. 46(9), pp 777–781, 2016

[6] Z. N. Sokolova, D. A. Veselov, N. A. Pikhtin, I. S. Tarasov and L. V. Asryan, "Increase in the internal optical loss with increasing pump current and the output power of quantum well lasers", *Semiconductors*, Vol. 51(7), 959–964, 2017

[7] E. A. Viktorov, Paul Mandel, "Electron-hole asymmetry and two-state lasing in quantum dot lasers" , Appl. Phys. Lett. 87, 053113 (2005)

Conclusions

Our primary objective was to theoretically analyze the DTI QD laser design and this was done by analyzing the effect of out-tunneling leakage of carriers from QDs in limiting the modulation bandwidth of a DTI QD laser and by analyzing the effect of electron-hole asymmetry on the device characteristics. We are confronted with results of significant relevance.

It can be noted (from plots of modulation bandwidth vs j on increasing w_{out}) that there is low relative reduction in modulation bandwidth i.e. out-tunneling does not sufficiently reduce the effectiveness of such a DTI design. Further, for higher out-tunneling coefficients, the relative drop in modulation bandwidth saturates and approaches a constant value. We then find that even for the worst case scenario i.e. in the case of resonant out-tunneling, relative reduction in modulation bandwidth for a DTI QD laser remains low.

From this, we draw a reasonable and commercially significant conclusion, that the DTI QD laser is a fairly robust device in terms of sensitivity to out-tunneling leakage i.e. much effort need not be paid in suppressing this phenomenon.

On analyzing the effect of electron-hole asymmetry on the device characteristics of a DTI QD laser, it can be noted (from plots of modulation bandwidth vs injection current) that there is no reduction in the maximum modulation bandwidth *i.e. electron-hole asymmetry does not indicate a reduction in the effectiveness of such a DTI design.* This is because the maximum modulation bandwidth depends on both, the effective differential non-stimulated recombination time as well the photon lifetime in the optical cavity. The photon lifetime being much much smaller than the former is the dominating factor, and hence we see no appreciable change in the maximum modulation bandwidth.

In the course of this analysis, we also see that the actual condition i.e. that of electron hole asymmetry is closer, among the cases of symmetry, to symmetry assuming hole parameters rather than electron parameters. As such, in cases where electron-hole symmetry must be used (in order to facilitate numerical simplifications), a recommendation of this study would be to use hole parameters instead of electron parameters.